RM L9K04

NACA RM L9K04

NACA

RESEARCH MEMORANDUM

LOW-SPEED INVESTIGATION OF THE AERODYNAMIC LOADS ON THE DROOP-NOSE FLAP OF A WING WITH LEADING EDGE SWEPT BACK 47.5° AND HAVING SYMMETRICAL CIRCULAR-ARC AIRFOIL SECTIONS AT A REYNOLDS NUMBER OF 4.3×10^6

By Edward F. Whittle, Jr., and Marvin P. Fink

Langley Aeronautical Laboratory
Langley Air Force Base, Va.

NATIONAL ADVISORY COMMITTEE FOR AERONAUTICS

WASHINGTON
January 16, 1950

NATIONAL ADVISORY COMMITTEE FOR AERONAUTICS

RESEARCH MEMORANDUM

LOW-SPEED INVESTIGATION OF THE AERODYNAMIC LOADS ON THE DROOP-NOSE FLAP OF A WING WITH LEADING EDGE SWEPT BACK 47.5° AND HAVING SYMMETRICAL CIRCULAR-ARC AIRFOIL SECTIONS AT A REYNOLDS NUMBER OF 4.3×10^6

By Edward F. Whittle, Jr., and Marvin P. Fink

SUMMARY

An investigation has been made in the Langley full-scale tunnel at a Reynolds number of 4.3×10^6 and a Mach number of 0.07 of the pressure distribution on the full-span droop-nose flap of a wing with the leading edge swept back 47.5° and having symmetrical circular-arc airfoil sections. Flap pressure distributions were obtained for the basic configuration, the full-span droop-nose flap deflected 10°, 20°, 30°, and 40°, the semispan plain flap deflected 40°, and the full-span droop-nose flap deflected 40° in combination with the semispan plain flap deflected 40°.

The loading on the undeflected droop-nose flap generally shifted inboard with increasing angle of attack. Deflecting the droop-nose flap reduced the loading on the inboard sections and increased the loading on the outboard sections so that, at a given angle of attack, the center of pressure was shifted outboard and rearward. Deflecting the plain flap 40° in combination with the droop-nose flap either undeflected or deflected had no appreciable effect on either the character of the loading produced by the droop-nose flap or the center-of-pressure location.

The maximum flap normal-force and hinge-moment coefficients of 1.98 and 0.85, respectively, were attained for the configuration with the droop-nose flap deflected 40°. Calculations indicate that the hinge moment of this droop-nose flap would not be excessive in the normal landing-approach condition for this sweptback wing.

INTRODUCTION

Wings being designed for high-speed flight are incorporating thin airfoil sections and large angles of sweep, which usually result in low maximum lift coefficients and poor stalling characteristics. The application of leading-edge high-lift devices has been shown to be effective in providing an improvement in the low-speed characteristics. Accordingly, interest has been expressed regarding the aerodynamic loads on leading-edge flaps in the landing-flight regime. Some two-dimensional data on a droop-nose flap are presented in reference 1. Some three-dimensional results for a partial-span extensible leading-edge flap (reference 2) and a partial-span droop-nose flap (reference 3) are currently available but, in general, few experimental data are available concerning the loading on the leading-edge flaps of sweptback wings.

Although the difference between the leading-edge sweep of the wings of references 3 and 4 was not large, it was believed that the greater intensity of the leading-edge separation on the wing of reference 4 would influence the droop-nose-flap loading. Therefore, the pressure distributions on the full-span droop-nose flap of the wing of reference 4 were determined and are reported in this paper. The tests were conducted in the Langley full-scale tunnel with and without a plain flap deflected 40° at a Reynolds number of 4.3×10^6 and a Mach number of 0.07.

SYMBOLS

C_L wing lift coefficient $\left(\frac{\text{Lift}}{qS}\right)$

P pressure coefficient $\left(\frac{p - p_o}{q}\right)$

P_R resultant pressure coefficient $\left(P_{lower} - P_{upper}\right)$

c_{n_f} droop-nose-flap section normal-force coefficient,

$$\int_0^1 P_R \, d\left(\frac{x_f}{c_f}\right)$$, positive when force is up

c_{h_f} droop-nose-flap section hinge-moment coefficient,

$$\int_0^1 P_R \frac{x_f}{c_f} d\left(\frac{x_f}{c_f}\right)$$, positive when flap tends to deflect upward

C_{N_f} droop-nose-flap normal-force coefficient,

$$\int_0^1 c_{n_f} \frac{c_f}{c_f'} d\left(\frac{y_f}{b_f}\right)$$, positive when force is up

C_{h_f} droop-nose-flap hinge-moment coefficient,

$$\int_0^1 c_{h_f}\left(\frac{c_f}{\bar{c}_f}\right)^2 d\left(\frac{y_f}{b_f}\right)$$, positive when flap tends to deflect upward

$(C.P.)_{x_f}$ chordwise location of the flap center of pressure, percent flap chord from the leading edge

$(C.P.)_{y_f}$ spanwise location of the flap center of pressure, percent flap span from the inboard end

p local static pressure

p_o free-stream static pressure

q free-stream dynamic pressure

S wing area

W/S wing loading

x_f chordwise coordinate measured from and normal to the hinge line

c_f local chord of droop-nose flap, normal to the hinge line

c_f' mean chord of droop-nose flap, normal to the hinge line

$\bar{c}_f$ root-mean-square chord of droop-nose flap, normal to the hinge line

c'	chord perpendicular to the line of maximum thickness
y_f	spanwise coordinate, measured from the inboard end of the flap and along the hinge line
b_f	span of the droop-nose flap, measured along the hinge line
α	angle of attack, degrees
δ_n	full-span droop-nose-flap deflection, degrees
δ_f	semispan-plain-flap deflection, degrees
V	forward velocity, miles per hour

MODEL AND TESTS

Model.- The wing model used for this investigation had the leading-edge swept back 47.5°, 10-percent-thick symmetrical circular-arc airfoil sections perpendicular to the line of maximum thickness, an aspect ratio of 3.5, and a taper ratio of 0.5. The full-span droop-nose flap and semispan plain flap had chords which were 20 percent of the wing chord measured perpendicular to the line of maximum thickness. The detailed geometric characteristics of the wing equipped with these flaps are shown in figure 1.

The flaps were hinged at the lower surface, and when deflected, the gap in the upper surface was sealed and faired to the wing contour. The upper and lower surfaces of the full-span droop-nose flap were fitted with pressure orifices which were arranged in chordwise rows perpendicular to the hinge line of the flap. These chordwise and spanwise locations of pressure orifices are shown in figure 2. Orifices were not installed on the fairing.

Tests.- The tests were made over a large angle-of-attack range at a Reynolds number of 4.3×10^6 and a Mach number of 0.07. The configurations tested included the basic wing, the wing with (a) the semispan plain flap deflected 40°, (b) the full-span droop-nose flap deflected 10°, 20°, 30°, and 40°, and with (c) the semispan plain flap deflected 40° in combination with the full-span droop-nose flap deflected 40°. The pressures on the upper and lower surfaces of the full-span droop-nose flap were measured on a multiple-tube manometer and photographically recorded.

PRESENTATION OF DATA

The selection of a full-span droop-nose flap was based on the results of reference 5. These results showed that although a full-span droop-nose flap produced a tendency for static longitudinal instability at maximum lift, it produced a more linear pitching-moment curve up to maximum lift, a higher maximum lift coefficient, and more favorable lift-drag ratio characteristics near maximum lift than did a partial-span droop-nose flap.

The configurations tested were the droop-nose flap deflected 0°, 10°, 20°, 30°, and 40°, the plain flap deflected 40°, and the droop-nose flap deflected 40° in combination with the plain flap deflected 40°. In order to facilitate the analysis of the data for the configurations showing the greatest effects on the flap loading characteristics, only the data for the droop-nose flap deflected 0° and 40°, the plain flap deflected 40°, and the droop-nose flap deflected 40° in combination with the plain flap deflected 40° are presented in the figures. The basic data for droop-nose-flap deflections of 10°, 20°, and 30° are given in tables I, II, and III. The variations of lift coefficient with angle of attack for the various configurations are presented in figure 3. The pressure distributions on the droop-nose flap are given in figures 4 to 7 and the variations of the section normal-force and hinge-moment coefficients with angle of attack are shown in figure 8. The spanwise variations of the loading parameters are presented in figures 9 to 12. The effect of various angles of droop-nose-flap deflection on the spanwise loading parameters at two angles of attack is given in figure 13. The variation of the flap normal-force and hinge-moment coefficients with angle of attack is given in figure 14, and the spanwise and chordwise variations of the center-of-pressure locations with angle of attack are presented in figure 15. The variation of the calculated flap hinge moment with airspeed for three landing configurations is shown in figure 16.

The data have been corrected for the support tares, the blocking effect, stream alinement, and the jet-boundary effect calculated on the basis of an unswept wing. Since representative calculations showed the chordwise-force coefficient to be of the order of 1 percent of the normal-force coefficient, the chordwise-force coefficient was neglected in determining the hinge-moment coefficients.

RESULTS AND DISCUSSION

Flow and Section Characteristics

The flap chordwise pressure distributions for the undeflected flap (fig. 4) show the characteristic peak-negative-pressure concentration at the leading edge for the most inboard station. As indicated by the movement of the negative-pressure "bump" with increasing angle of attack, the separation vortex is shown to move rapidly spanwise and rearward from the flap leading edge. This phenomenon is discussed in detail in reference 4. Since the deflection of the plain flap (fig. 5) has mainly the effect of increasing the section lift at a given angle of attack, the chordwise distribution of pressures is essentially the same as for the neutral flap configuration. Deflection of the droop-nose flap (fig. 6) effectively introduces a large local camber increase at the leading edge which reduces the tendency for early flow separation and development of the leading-edge separation vortex. In general, wherever comparison can be made, the pressure distributions presented in this paper (figs. 4 to 7) are similar to those for the deflected flap of the 42° sweptback wing of reference 3, and for this reason it is believed that with the flap deflected a similar type of flow occurs for both plan forms.

In order to show more clearly the over-all droop-nose-flap section characteristics, the flap section normal-force and hinge-moment coefficients are presented as functions of angle of attack (fig. 8). Deflecting the plain flap 40° causes tip stall to move progressively inboard at a lower angle of attack and deflecting the droop-nose flap 40° delays the inboard progression of tip stall, as compared to the basic unflapped configuration. Inasmuch as the stalling of this thin swept wing is characterized by leading-edge separation, the leading-edge flap has a pronounced influence on the control of tip stall when deflected in combination with the plain flap. Except for the most outboard sections, none of the flap sections has attained its maximum loading condition at the highest angle of attack tested ($\alpha = 21.5^\circ$).

Spanwise Loading Parameters and Center-of-Pressure Variation

The basic configuration (fig. 9) shows an almost uniform spanwise loading distribution for angles of attack up to 6.6°, beyond which the most outboard section ($0.882b_f$) stalls. With increasing angle of attack, there is no further increase in load on the outboard sections, but there is an increase in load on the inboard sections until, at an angle of attack of 18.0°, the $0.064b_f$ section is carrying its maximum load. The flap spanwise and chordwise center-of-pressure locations vary between 33 and 44 percent of the flap span and 50 and 55 percent of the flap chord, respectively (fig. 15). Deflecting the plain flap 40° increases the loading for a given angle of attack, but has no appreciable effect on either the characteristic loading (fig. 10) or the spanwise and chordwise center-of-pressure locations (fig. 15) in the high angle-of-attack range.

Deflecting the droop-nose flap 40° (fig. 11) produces a change in the characteristic loading over the droop-nose flap. The delay of leading-edge separation and the delay of tip stall (fig. 6) reduce the loading on the inboard sections and enable the outboard sections to carry more load than the corresponding undeflected flap sections (figs. 9 and 11), so that, at a given angle of attack, the center-of-pressure location shifts outboard and rearward (fig. 15). With the droop-nose flap deflected 40°, the spanwise center-of-pressure location varies from 50 to 43 percent of the flap span (fig. 15) and the chordwise center-of-pressure location varies from 77 to 57 percent of the flap chord between angles of attack of 14.4° and 25.8°, respectively (fig. 15).

The effect of droop-nose-flap deflection on the spanwise flap loading for angles of attack of approximately 14.2° and 23.8° is presented in figure 13. In general, increasing the droop-nose-flap deflection progressively decreases the loading over the inboard flap sections and increases the loading over the outboard flap sections. For the angle of attack of 23.8° (fig. 13), the data for a droop-nose-flap deflection of 10° show that all sections are stalled at this angle of attack. For a given angle of attack, progressive increases in droop-nose-flap deflection cause the spanwise and chordwise center-of-pressure locations to shift outboard and rearward, respectively (fig. 15).

The addition of the plain flap deflected 40° in combination with the droop-nose flap deflected 40° (fig. 12) increases the magnitude of the loading for a given angle of attack, but has no effect on the character of the loading developed by the droop-nose flap (fig. 11). Neither the spanwise nor chordwise center-of-pressure locations (fig. 15) are appreciably affected by the addition of the plain flap.

The characteristic loadings on the partial-span droop-nose flap of reference 3 are similar to those presented in this paper, which indicates that these data represent generally the droop-nose-flap loadings for wings in the sweep range of 45° and having thin sharp-edge sections.

Flap Normal-Force and Hinge-Moment Coefficients

The flap maximum normal-force and hinge-moment coefficients for the basic configuration are 1.72 and 0.80, respectively, at an angle of attack of 16.0° (fig. 14). Deflecting the plain flap 40° increased the flap normal-force and hinge-moment coefficients for a given angle of attack but reduced their maximum values to 1.62 and 0.78, respectively, at an angle of attack of about 14.0°. With the droop-nose flap deflected 40°, the flap normal-force and hinge-moment coefficients are reduced by about 1.00 and 0.62, respectively, as compared to the undeflected flap for a given angle of attack, but their maximum values are increased to 1.98 and 0.85, respectively, at an angle of attack of about 26°. The combination of the two flaps deflected 40° reduced the flap normal-force and hinge-moment coefficients by about 0.72 and 0.48, respectively, for a given angle of attack. Maximum flap normal-force and hinge-moment coefficients were not attained, but it appears that larger maximum values than for any other configuration tested would be attained at angles of attack greater than 21.5°.

In order to obtain an estimate of the hinge moments which an actuating mechanism would be required to overcome, when deflecting and raising the droop-nose flap for various landing configurations, the flap hinge moments about the hinge axis are presented for a wing loading of 40 pounds per square foot for three landing configurations (fig. 16). From this information it is clearer than from the basic hinge-moment coefficient plots that there is a relatively rapid load reduction as the droop-nose flap is deflected in the landing approach and then a load increase as the flight speed is reduced. The magnitude of the maximum hinge moment should not be excessive for the usual mechanical flap-actuating systems.

CONCLUDING REMARKS

The results of an investigation to determine the pressure distribution on the droop-nose flap of a wing with the leading edge swept back 47.5° and having symmetrical circular-arc airfoil sections indicate the following:

1. The loading on the undeflected droop-nose flap generally shifted inboard with increasing angle of attack. Deflecting the droop-nose flap reduced the loading on the inboard sections and increased the loading on the outboard sections, so that, at a given angle of attack, the center of pressure was shifted outboard and rearward.

2. Deflecting the plain flap 40° in combination with the droop-nose flap either undeflected or deflected had no appreciable effect on either the character of the loading produced by the droop-nose flap or the center-of-pressure location.

3. The maximum flap normal-force and hinge-moment coefficients of 1.98 and 0.85, respectively, were attained for the configuration with the droop-nose flap deflected 40°.

4. Calculations show that the maximum droop-nose-flap hinge moments developed in the landing-flight range should not be difficult to control by the usual flap-operating systems.

Langley Aeronautical Laboratory
National Advisory Committee for Aeronautics
Langley Air Force Base, Va.

REFERENCES

1. Underwood, William J., and Nuber, Robert J.: Aerodynamic Load Measurements over Leading-Edge and Trailing-Edge Plain Flaps on a 6-Percent-Thick Symmetrical Circular-Arc Airfoil Section. NACA RM L7H04, 1947.

2. Salmi, Reino J.: Pressure-Distribution Measurements over an Extensible Leading-Edge Flap on Two Wings Having Leading-Edge Sweep of 42° and 52°. NACA RM L9A18, 1949.

3. Spooner, Stanley H., and Woods, Robert L.: Low-Speed Pressure Distributions over the Drooped-Nose Flap of a 42° Sweptback Wing with Circular-Arc Airfoil Sections at a Reynolds Number of 5.3×10^6. NACA RM L8F16, 1948.

4. Lange, Roy H., Whittle, Edward F., Jr., and Fink, Marvin P.: Investigation at Large Scale of the Pressure Distribution and Flow Phenomena over a Wing with the Leading Edge Swept Back 47.5° Having Circular-Arc Airfoil Sections and Equipped with Drooped-Nose and Plain Flaps. NACA RM L9G15, 1949.

5. Guryansky, Eugene R., and Lipson, Stanley: Effect of High-Lift Devices on the Longitudinal and Lateral Characteristics of a 45° Sweptback Wing with Symmetrical Circular-Arc Sections. NACA RM L8D06, 1948.

TABLE I.– FLAP PRESSURE COEFFICIENTS FOR THE DROOP–NOSE FLAP DEFLECTED

(a) $\delta_n = 10^\circ$

	$\frac{x_f}{c_f}$ \ $\frac{y_f}{b_f}$	$\alpha = 4.9^\circ$					$\alpha = 8.6^\circ$				
		0.064	0.264	0.467	0.675	0.882	0.064	0.264	0.467	0.675	0.882
Upper surface	1.9		–0.38					–0.95			
	5.0	0.01	–.47	–0.24	–0.32	–0.39	–0.74	–1.05	–0.79	–0.80	–0.80
	10.0	.20	–.10	–.12	–.15		–.70	–1.05	–.84	–.80	
	20.0	.10	–.05	–.09		–.10	–.96	–1.16	–.89		–.86
	30.0	.06	–.09	–.09	–.14	–.15	–.05	–.89	–.94	–.80	–.80
	50.0	–.15		–.16	–.19	–.19	–.20		–.81	–.75	–.66
	70.0	–.10	–.23	–.24	–.25	–.27	–.28	–.40	–.56	–.61	–.42
	90.0	.20	–.38	–.38	–.39		.25	–.50	–.49	–.51	
Lower surface	10.0	.26	.30	.26	.20	.20	.44	.45	.45	.36	.34
	50.0	.20	.20	.19	.10	.12	.34	.30	.31	.24	.21
	90.0	.28	.22			.12	.36	.30			.17

	$\frac{x_f}{c_f}$ \ $\frac{y_f}{b_f}$	$\alpha = 12.3^\circ$					$\alpha = 14.2^\circ$				
		0.064	0.264	0.467	0.675	0.882	0.064	0.264	0.467	0.675	0.882
Upper surface	1.9		–1.14					–1.34			
	5.0	–1.20	–1.25	–1.05	–0.97	–0.69	–1.64	–1.34	–1.14	–0.89	–0.57
	10.0	–1.24	–1.23	–1.11	–1.00		–1.69	–1.43	–1.21	–.89	
	20.0	–1.93	–1.31	–1.17		–.70	–2.51	–1.51	–1.28		–.58
	30.0	–.76	–1.44	–1.17	–.98	–.70	–1.90	–1.63	–1.30	–.90	–.58
	50.0	–.31		–1.27	–1.00	–.70	–.41		–1.36	–.90	–.58
	70.0	–.37	–.99	–1.31	–1.00	–.71	–.46	–1.63	–1.44	–.90	–.58
	90.0	.34	–.58	–1.12	–.72		.35	–.97	–1.46	–.97	
Lower surface	10.0	.57	.52	.50	.40	.40	.62	.55	.53	.44	.43
	50.0	.46	.41	.40	.31	.30	.53	.46	.45	.36	.35
	90.0	.47	.39			.25	.55	.44			.27

	$\frac{x_f}{c_f}$ \ $\frac{y_f}{b_f}$	$\alpha = 19.9^\circ$					$\alpha = 23.8^\circ$				
		0.064	0.264	0.467	0.675	0.882	0.064	0.264	0.467	0.675	0.882
Upper surface	1.9		–1.53					–1.30			
	5.0	–2.56	–1.68	–1.01	–0.73	–0.46	–2.97	–1.41	–1.04	–0.72	–0.40
	10.0	–2.60	–1.63	–1.10	–.73		–2.87	–1.39	–1.06	–.72	
	20.0	–2.99	–1.69	–1.17		–.48	–3.24	–1.44	–1.06		–.41
	30.0	–4.57	–1.78	–1.19	–.75	–.48	–4.78	–1.48	–1.08	–.74	–.44
	50.0	–.45	–.89	–1.24	–.76	–.48	–.59	–.82	–1.08	–.74	–.44
	70.0	–.62	–2.30	–1.29	–.76	–.50	–.70	–1.59	–1.08	–.74	–.44
	90.0	.41	–2.16	–1.38	–1.64		.44	–1.63	–1.10	–1.18	
Lower surface	10.0	.68	.53	.57	.46	.45	.71	.55	.53	.46	.45
	50.0	.66	.55	.56	.44	.40	.75	.61	.57	.46	.43
	90.0	.65	.51			.33	.73	.58			.35

NACA

TABLE I.– Continued

(b) $\delta_n = 20^\circ$

	x_f/c_f \ y_f/b_f	α = 4.9°					α = 10.5°				
		0.064	0.264	0.467	0.675	0.882	0.064	0.264	0.467	0.675	0.882
Upper surface	1.9		0.40					−0.66			
	5.0	0.49	.24	0.26	0.19	0.24	−0.30	−.75	−0.75	−0.82	−0.80
	10.0	.40	.21	.20	.15		−.10	−.76	−.85	−.82	
	20.0	.33	.14	.10		.11	0	−.34	−.89		−.85
	30.0	.25	.07	.05	.01	.05	−.03	−.25	−.76	−.76	−.63
	50.0	.09		−.08	−.09	−.06	−.16		−.37	−.52	−.45
	70.0	−.03	−.16	−.21	−.21	−.21	−.27	−.45	−.47	−.50	−.49
	90.0	−.19	−.41	−.45	−.44		−.43	−.74	−.75	−.69	
Lower surface	10.0	−.27	−.05	.12	0	−.14	.34	.39	.44	.34	.34
	50.0	.15	.13	.19	.06	.08	.33	.30	.35	.23	.25
	90.0	.32	.21			.13	.44	.35			.25

	x_f/c_f \ y_f/b_f	α = 14.2°					α = 16.2°				
		0.064	0.264	0.467	0.675	0.882	0.064	0.264	0.467	0.675	0.882
Upper surface	1.9		−1.30					−1.35			
	5.0	−0.99	−1.39	−1.29	−1.23	−1.11	−1.12	−1.45	−1.50	−1.35	−0.92
	10.0	−.99	−1.36	−1.29	−1.23		−1.17	−1.44	−1.54	−1.35	
	20.0	−1.52	−1.45	−1.34		−1.11	−1.86	−1.53	−1.59		−.95
	30.0	−.27	−1.41	−1.40	−1.24	−1.13	−.66	−1.62	−1.63	−1.36	−.96
	50.0	−.35		−1.35	−1.26	−1.15	−.36		−1.73	−1.36	−.96
	70.0	−.46	−.57	−.88	−1.15	−1.06	−.47	−.70	−1.51	−1.38	−.96
	90.0	−.60	−.83	−.74	−.97		−.64	−.79	−1.10	−1.31	
Lower surface	10.0	.54	.50	.52	.43	.41	.59	.54	.55	.43	.41
	50.0	.45	.41	.44	.34	.34	.51	.46	.46	.35	.38
	90.0	.53	.44			.31	.59	.46			.34

	x_f/c_f \ y_f/b_f	α = 19.9°					α = 23.8°				
		0.064	0.264	0.467	0.675	0.882	0.064	0.264	0.467	0.675	0.882
Upper surface	1.9		−1.74					−1.72			
	5.0	−1.83	−1.92	−1.68	−1.06	−0.57	−2.44	−1.87	−1.44	−0.84	−0.47
	10.0	−1.86	−1.87	−1.63	−1.06		−2.47	−1.78	−1.35	−.84	
	20.0	−2.50	−1.95	−1.66		−.58	−2.85	−1.88	−1.35		−.50
	30.0	−2.43	−2.09	−1.68	−1.06	−.60	−4.25	−1.96	−1.36	−.85	−.50
	50.0	−.48		−1.73	−1.05	−.60	−.50		−1.36	−.85	−.52
	70.0	−.63	−2.07	−1.83	−1.06	−.60	−.70	−2.26	−1.36	−.85	−.52
	90.0	−.80	−1.37	−1.87	−1.03		−.90	−2.08	−1.36	−.86	
Lower surface	10.0	.65	.54	.54	.45	.44	.74	.58	.54	.45	.45
	50.0	.59	.51	.53	.43	.40	.70	.60	.55	.44	.44
	90.0	.64	.51			.35	.74	.59			.40

NACA

TABLE I.— Concluded

(c) $\delta_n = 30^\circ$

	x_f/c_f \ y_f/b_f	α = 12.5°: 0.064	0.264	0.467	0.675	0.882	α = 18.2°: 0.064	0.264	0.467	0.675	0.882
Upper surface	1.9		−0.55					−1.39			
	5.0	0.33	−.65	−0.44	−0.60	−0.63	−0.80	−1.59	−1.39	−1.63	−1.39
	10.0	.25	−.54	−.55	−.60		−.81	−1.59	−1.48	−1.63	
	20.0	.20	−.15	−.36		−.45	−.90	−1.69	−1.54		−1.41
	30.0	.10	−.20	−.20	−.32	−.35	−.10	−1.45	−1.60	−1.63	−1.44
	50.0	−.10		−.35	−.37	−.44	−.35		−1.59	−1.60	−1.49
	70.0	−.25	−.51	−.55	−.55	−.61	−.50	−.70	−1.02	−1.39	−1.30
	90.0	−.50	−.90	−.95	−.90		−.75	−.12	−1.02	−1.14	
Lower surface	10.0	.22	.40	.41	.33	.30	.50	.55	.50	.44	.45
	50.0	.34	.35	.39	.26	.27	.50	.50	.45	.36	.40
	90.0	.54	.44			.30	.65	.55			.39

	x_f/c_f \ y_f/b_f	α = 20.0°: 0.064	0.264	0.467	0.675	0.882	α = 21.8°: 0.064	0.264	0.467	0.675	0.882
Upper surface	1.9		−1.67					−1.85			
	5.0	−1.06	−1.83	−1.68	−1.83	−1.24	−1.44	−2.01	−1.90	−1.75	−1.02
	10.0	−1.06	−1.79	−1.73	−1.83		−1.49	−1.96	−1.98	−1.73	
	20.0	−1.63	−1.92	−1.82		−1.25	−2.33	−2.07	−2.07		−1.04
	30.0	−.09	−1.92	−1.88	−1.83	−1.28	−.70	−2.21	−2.08	−1.78	−1.06
	50.0	−.40		−1.96	−1.89	−1.28	−.47		−2.21	−1.81	−1.06
	70.0	−.55	−.70	−1.55	−1.83	−1.25	−.64	−1.15	−2.07	−1.84	−1.10
	90.0	−.81	−1.11	−1.20	−1.55		−.90	−1.00	−1.63	−1.83	
Lower surface	10.0	.60	.59	.51	.45	.44	.65	.58	.51	.45	.45
	50.0	.55	.54	.50	.40	.40	.60	.55	.51	.44	.45
	90.0	.69	.56			.40	.71	.56			.44

	x_f/c_f \ y_f/b_f	α = 23.8°: 0.064	0.264	0.467	0.675	0.882
Upper surface	1.9		−2.02			
	5.0	−1.72	−2.16	−1.83	−1.25	−0.75
	10.0	−1.73	−2.12	−1.88	−1.25	
	20.0	−2.70	−2.21	−1.92		−.78
	30.0	−1.64	−2.36	−1.93	−1.29	−.78
	50.0	−.50		−2.02	−1.32	−.80
	70.0	−.70	−1.63	−2.06	−1.34	−.79
	90.0	−.97	−1.06	−1.92	−1.25	
Lower surface	10.0	.70	.56	.59	.50	.45
	50.0	.65	.56	.59	.48	.43
	90.0	.75	.58			.41

TABLE II.— FLAP SECTION NORMAL-FORCE AND HINGE-MOMENT

COEFFICIENTS FOR THE DROOP-NOSE FLAP DEFLECTED

$\delta_n = 10^\circ$

$\frac{y_f}{b_f}$ / α, deg	c_{n_f}					c_{h_f}				
	0.064	0.264	0.467	0.675	0.882	0.064	0.264	0.467	0.675	0.882
4.9	0.198	0.429	0.407	0.352	0.376	0.114	0.204	0.189	0.203	0.183
8.6	.457	.972	1.027	.935	.780	.255	.559	.577	.514	.478
12.3	1.000	1.523	1.614	1.247	.980	.686	.855	.819	.663	.505
14.2	1.397	1.940	1.798	1.243	.901	.955	1.029	.892	.630	.467
19.9	2.130	2.507	1.790	1.351	.878	1.464	1.198	.871	.599	.467
23.8	2.285	2.098	1.624	1.262	.823	1.567	1.034	.810	.590	.420

$\delta_n = 20^\circ$

$\frac{y_f}{b_f}$ / α, deg	c_{n_f}					c_{h_f}				
	0.064	0.264	0.467	0.675	0.882	0.064	0.264	0.467	0.675	0.882
4.9	−0.331	1.646	0.282	0.169	0.116	−0.225	0.007	0.063	0.016	−0.027
10.5	.358	.773	.958	.835	.836	.241	.374	.513	.472	.457
14.2	1.090	1.510	1.556	1.495	1.418	.593	.836	.868	.892	.739
16.2	1.257	1.585	1.952	1.695	1.289	.705	.896	1.041	.872	.653
19.9	1.832	2.435	2.283	1.472	.971	1.087	1.269	1.128	.749	.494
23.8	2.414	2.646	1.916	1.255	.912	1.470	1.303	.971	.630	.460

$\delta_n = 30^\circ$

$\frac{y_f}{b_f}$ / α, deg	c_{n_f}					c_{h_f}				
	0.064	0.264	0.467	0.675	0.882	0.064	0.264	0.467	0.675	0.882
12.5	0.428	0.830	0.891	0.792	0.825	0.102	0.363	0.404	0.382	0.385
18.2	.980	1.678	1.780	1.823	1.726	.509	.910	.960	.980	.911
20.0	1.552	2.143	1.439	2.241	1.525	.628	1.017	1.089	1.102	.806
21.8	1.831	2.411	2.555	1.766	1.185	.854	1.200	1.258	1.120	.759
23.8	1.225	1.836	2.068	2.098	1.598	1.041	1.333	1.280	.891	.601

TABLE III.– WING LIFT COEFFICIENTS AND FLAP NORMAL-FORCE AND HINGE-MOMENT PARAMETERS FOR THE DROOP-NOSE FLAP DEFLECTED

$\delta_n = 10^\circ$

α, deg	C_L \ y_f/b_f	$c_{n_f}(c_f/c_f')$					$c_{h_f}(c_f/\bar{c}_f)^2$				
		0.064	0.264	0.467	0.675	0.882	0.064	0.264	0.467	0.675	0.882
4.9	.21	0.266	0.510	0.431	0.311	0.280	0.156	0.216	0.158	0.118	0.076
8.6	.37	.615	1.111	1.045	.824	.579	.347	.592	.486	.300	.198
12.3	.58	1.298	1.705	1.643	1.057	.728	.932	.906	.689	.387	.209
14.2	.70	1.809	2.217	1.830	1.054	.669	1.249	1.049	.750	.368	.193
19.9	.85	2.758	2.865	1.822	1.145	.652	1.915	1.220	.732	.349	.193
23.8	.90	2.958	2.399	1.653	1.070	.611	2.049	1.054	.681	.345	.174

$\delta_n = 20^\circ$

α, deg	C_L \ y_f/b_f	$c_{n_f}(c_f/c_f')$					$c_{h_f}(c_f/\bar{c}_f)^2$				
		0.064	0.264	0.467	0.675	0.882	0.064	0.264	0.467	0.675	0.882
4.9	.18	-0.446	0.196	0.299	0.149	0.086	-0.305	-0.008	0.053	0.009	-0.011
10.5	.41	.751	.919	.976	.759	.621	.327	.396	.431	.276	.190
14.2	.60	1.411	1.726	1.584	1.268	1.013	.806	.886	.730	.465	.306
16.2	.65	1.628	1.812	1.987	1.437	.957	.958	.950	.876	.509	.270
19.9	.81	2.372	2.784	2.324	1.249	.721	1.421	1.293	.948	.437	.204
23.8	.88	3.126	3.024	1.951	1.065	.651	1.922	1.328	.817	.368	.191

$\delta_n = 30^\circ$

α, deg	C_L \ y_f/b_f	$c_{n_f}(c_f/c_f')$					$c_{h_f}(c_f/\bar{c}_f)^2$				
		0.064	0.264	0.467	0.675	0.882	0.064	0.264	0.467	0.675	0.882
12.5	.45	0.577	0.987	0.943	0.698	0.612	0.138	0.385	0.340	0.223	0.159
18.2	.66	1.269	1.918	1.812	1.546	1.233	.692	.964	.807	.572	.377
20.0	.79	1.649	2.183	2.190	1.851	1.186	.853	1.078	.916	.643	.334
21.8	.86	2.009	2.488	2.482	1.900	1.089	1.117	1.222	1.017	.654	.314
23.8	.90	2.371	2.755	2.601	1.459	.879	1.361	1.359	1.035	.520	.249

NACA

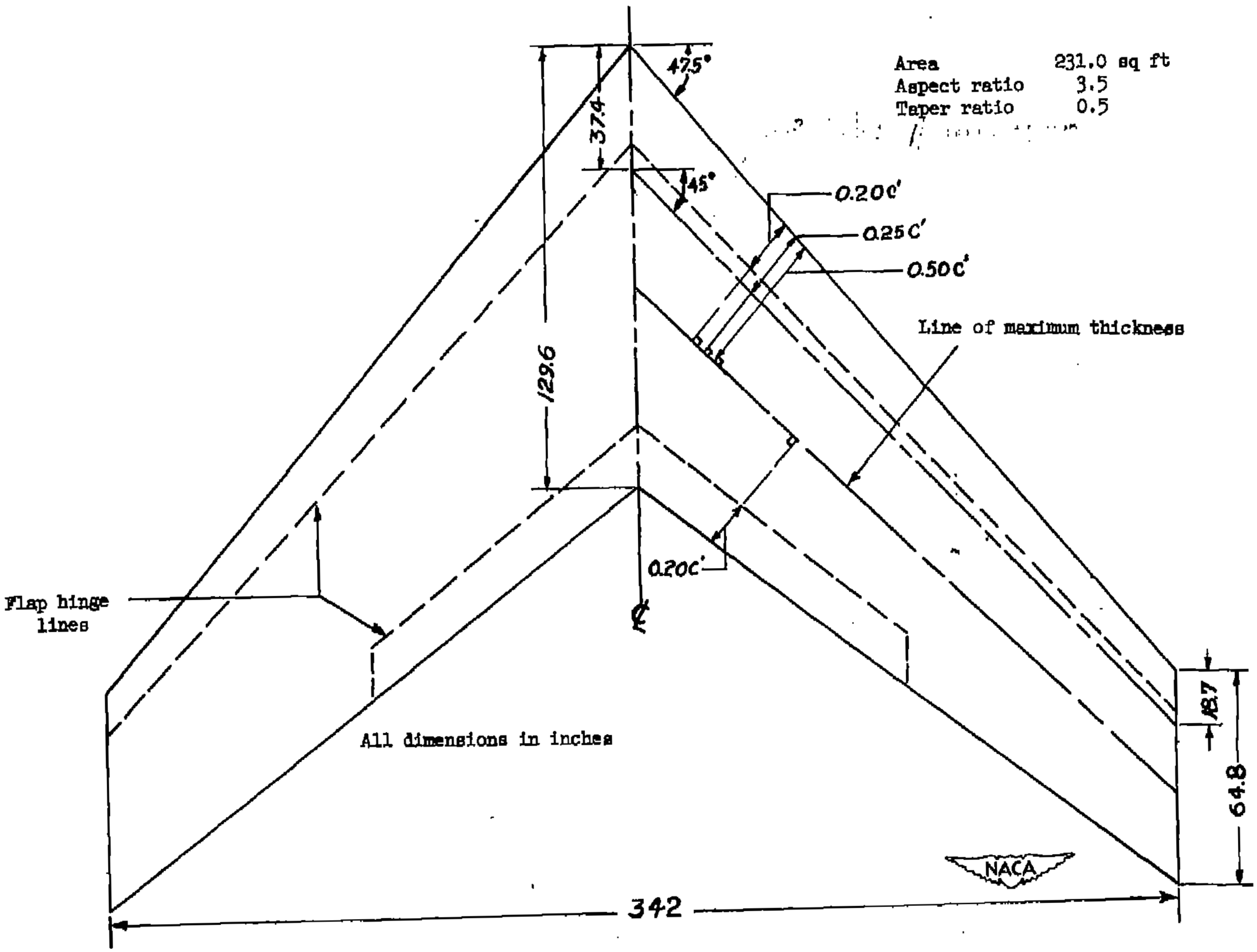

Figure 1.- Plan form of sweptback wing.

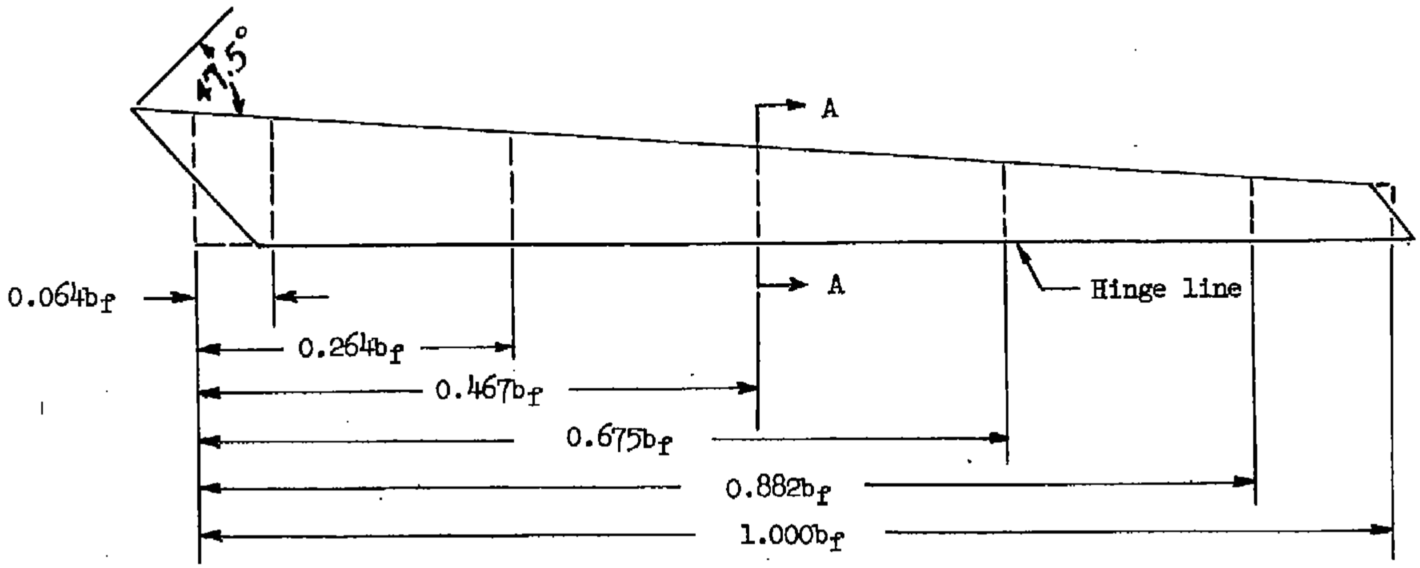

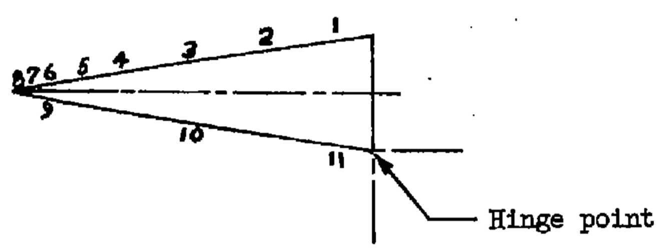

Section A-A

Orifice no.	$\frac{x_f}{c_f}$
1	90.0
2	70.0
3	50.0
4	30.0
5	20.0
6	10.0
7	5.0
8	1.9
9	10.0
10	50.0
11	90.0

NACA

Figure 2.- Spanwise and chordwise location of pressure orifices.

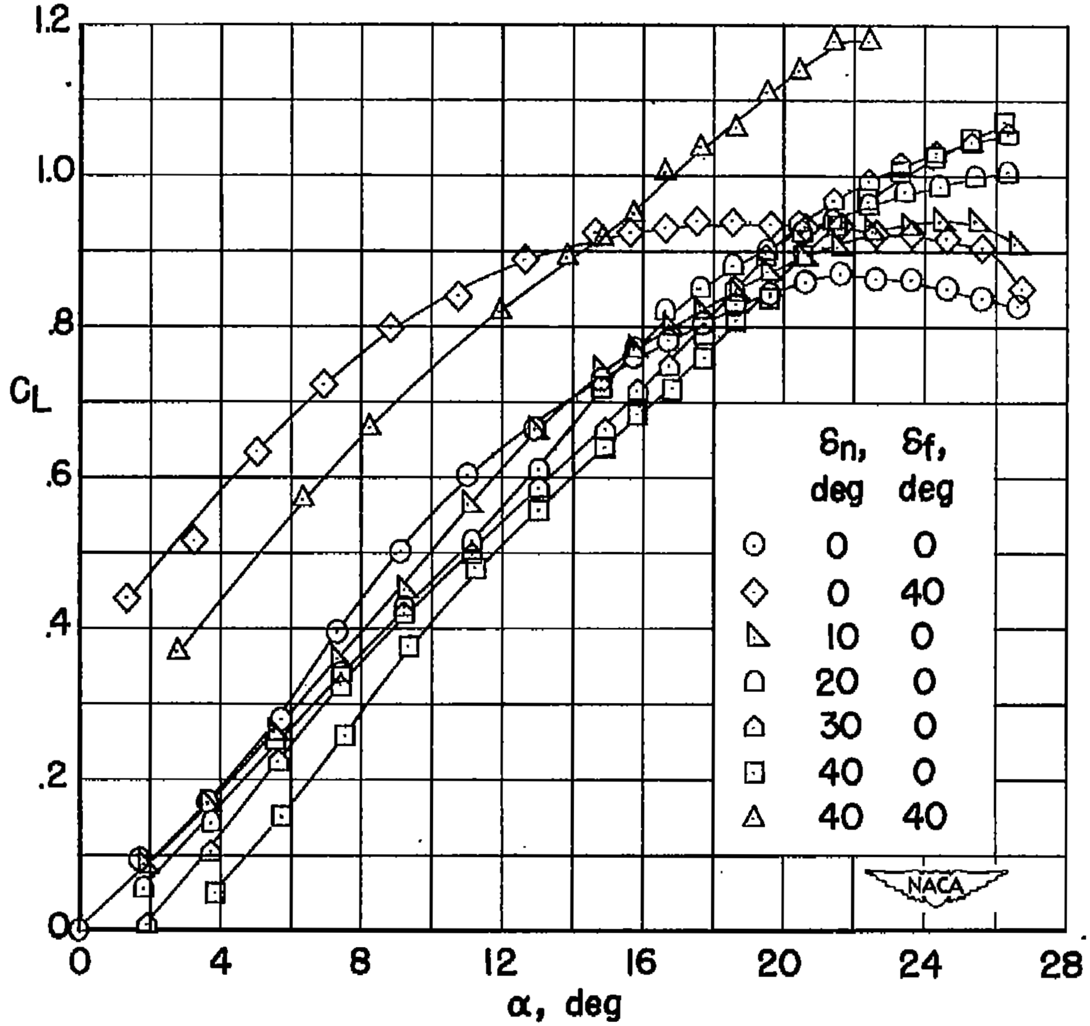

Figure 3.- Variation of lift coefficient with angle of attack for several flap configurations.

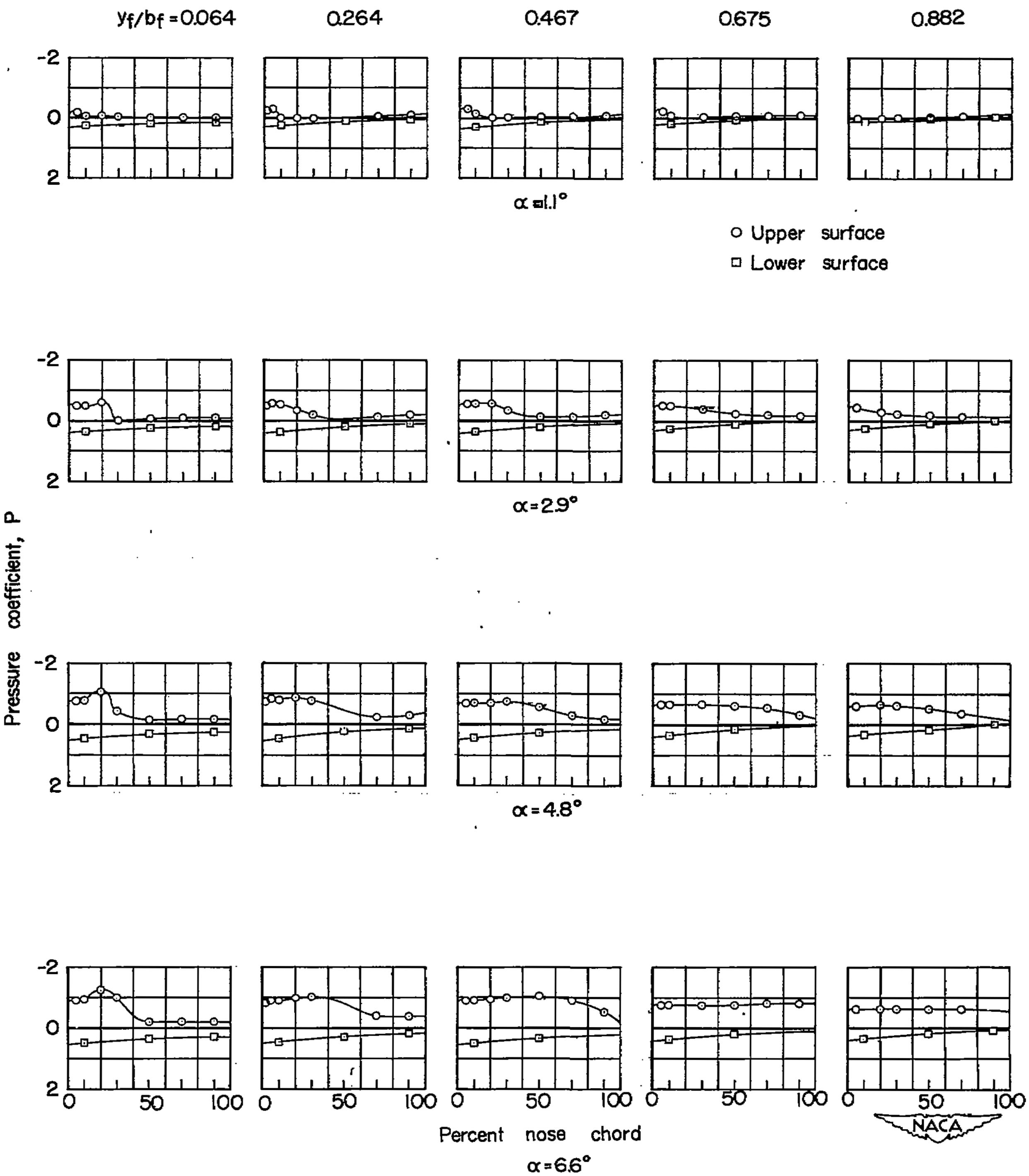

Figure 4.- Chordwise pressure distribution for five spanwise stations. Basic wing.

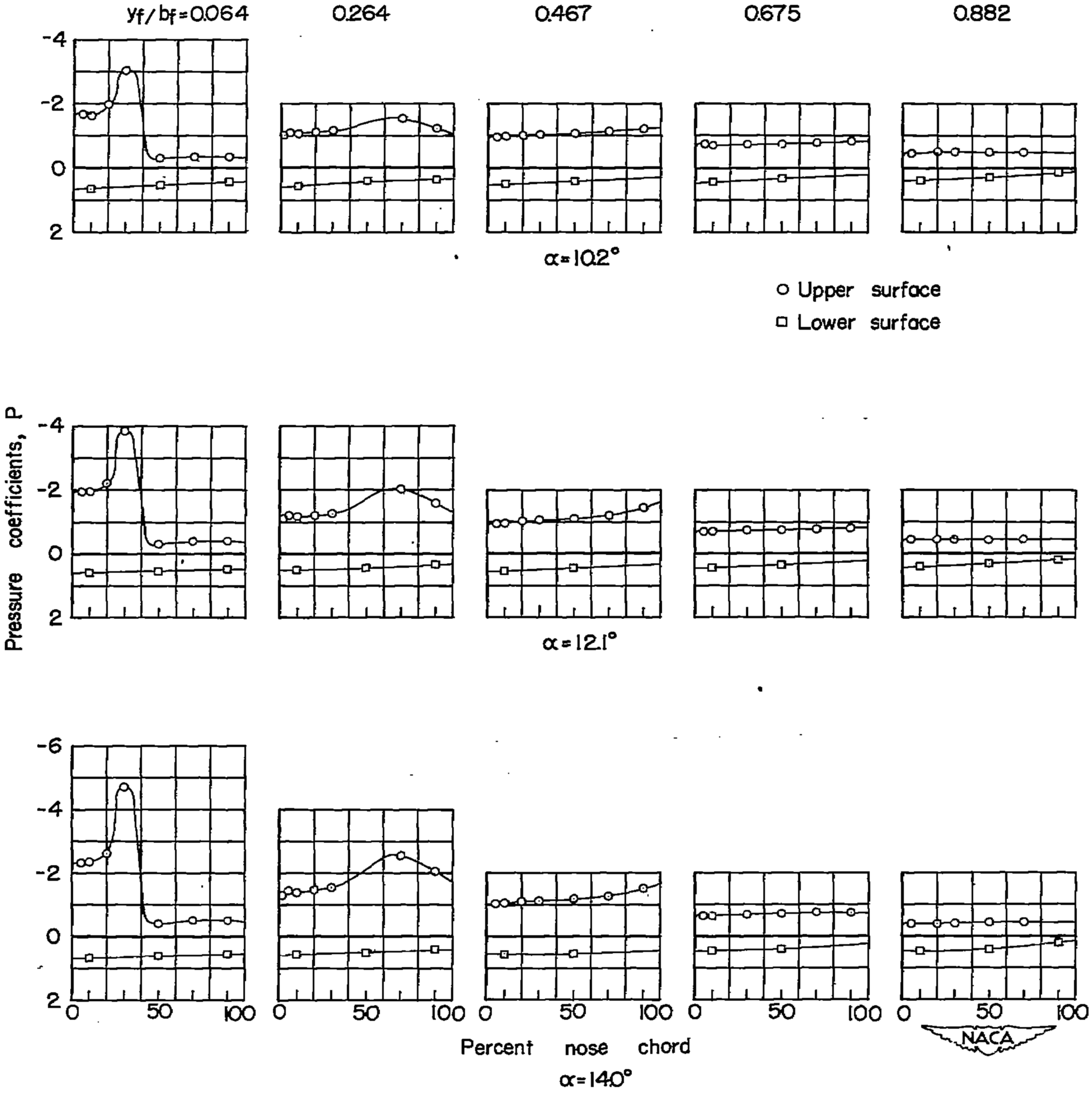

Figure 4.- Continued.

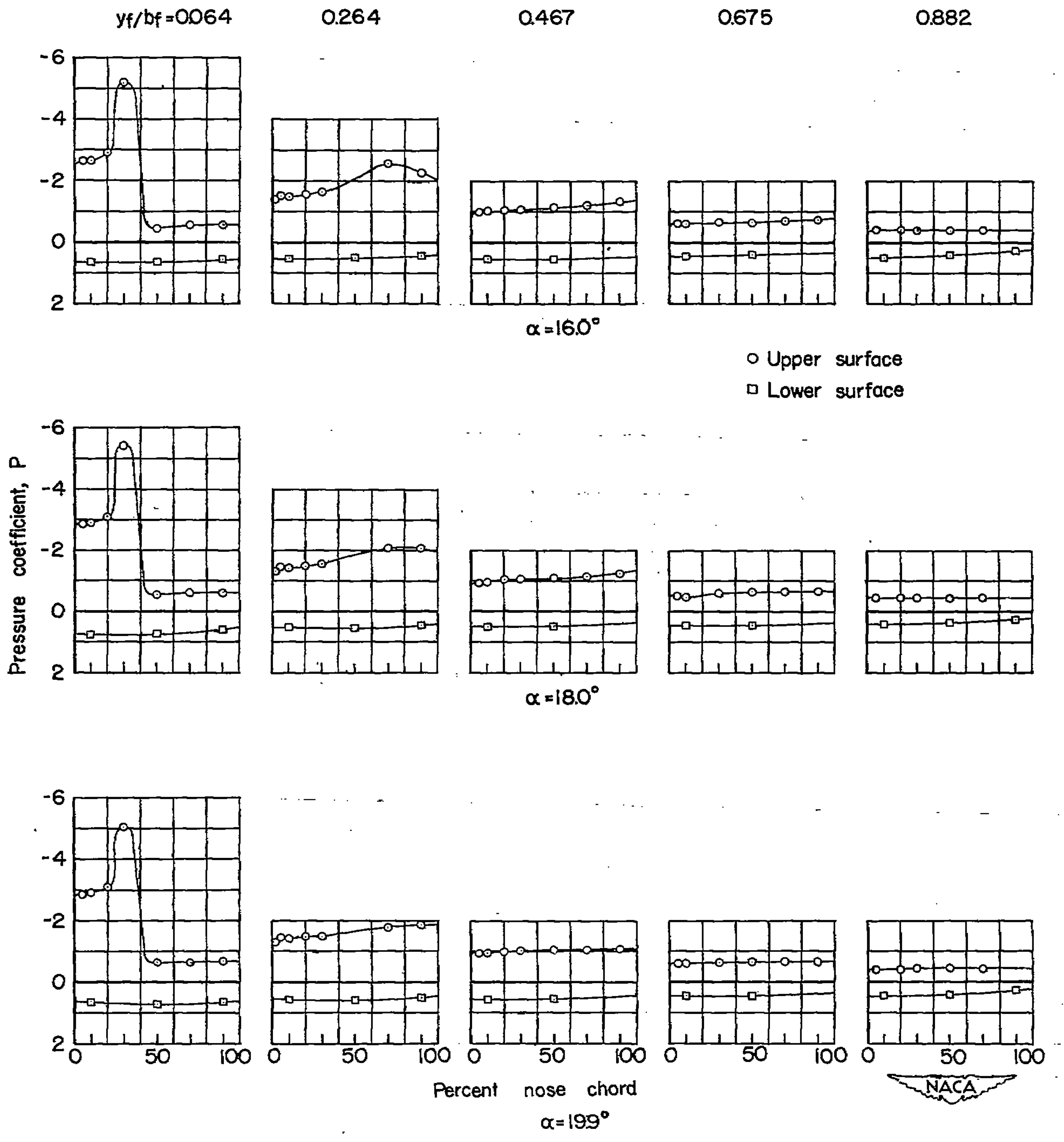

Figure 4.- Concluded.

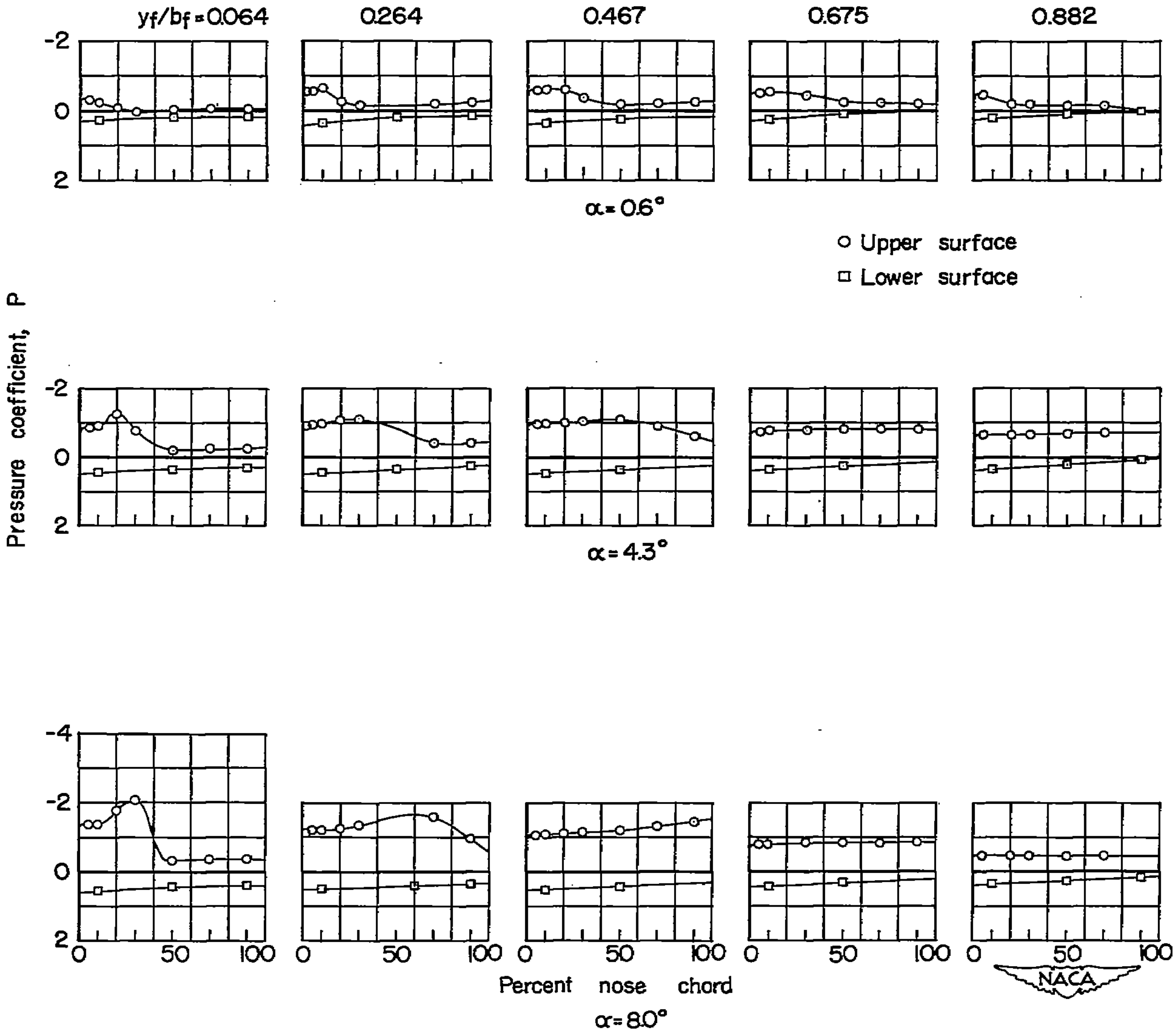

Figure 5.- Chordwise pressure distribution for five spanwise stations. Semispan plain flap deflected 40°.

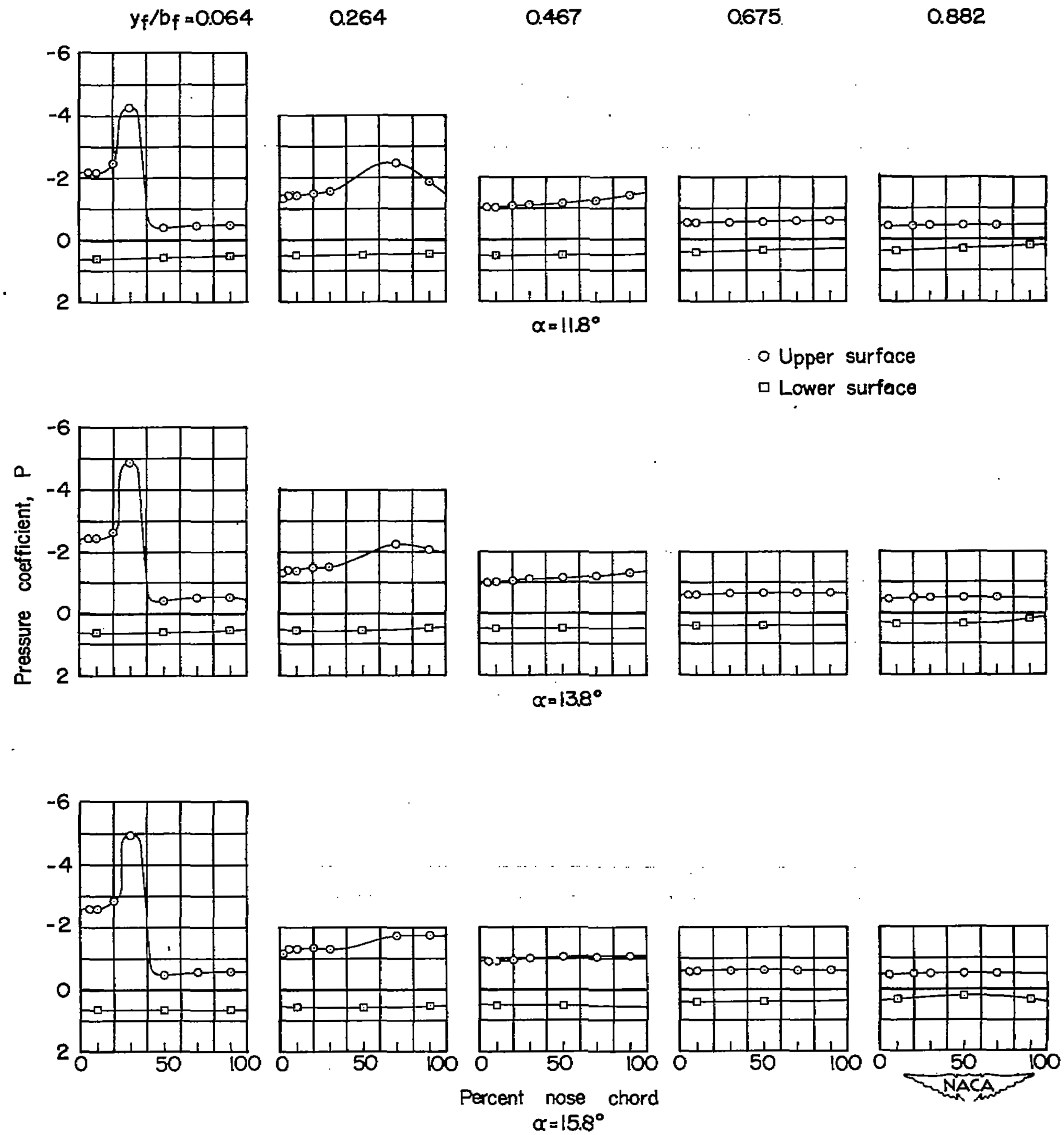

Figure 5.- Concluded.

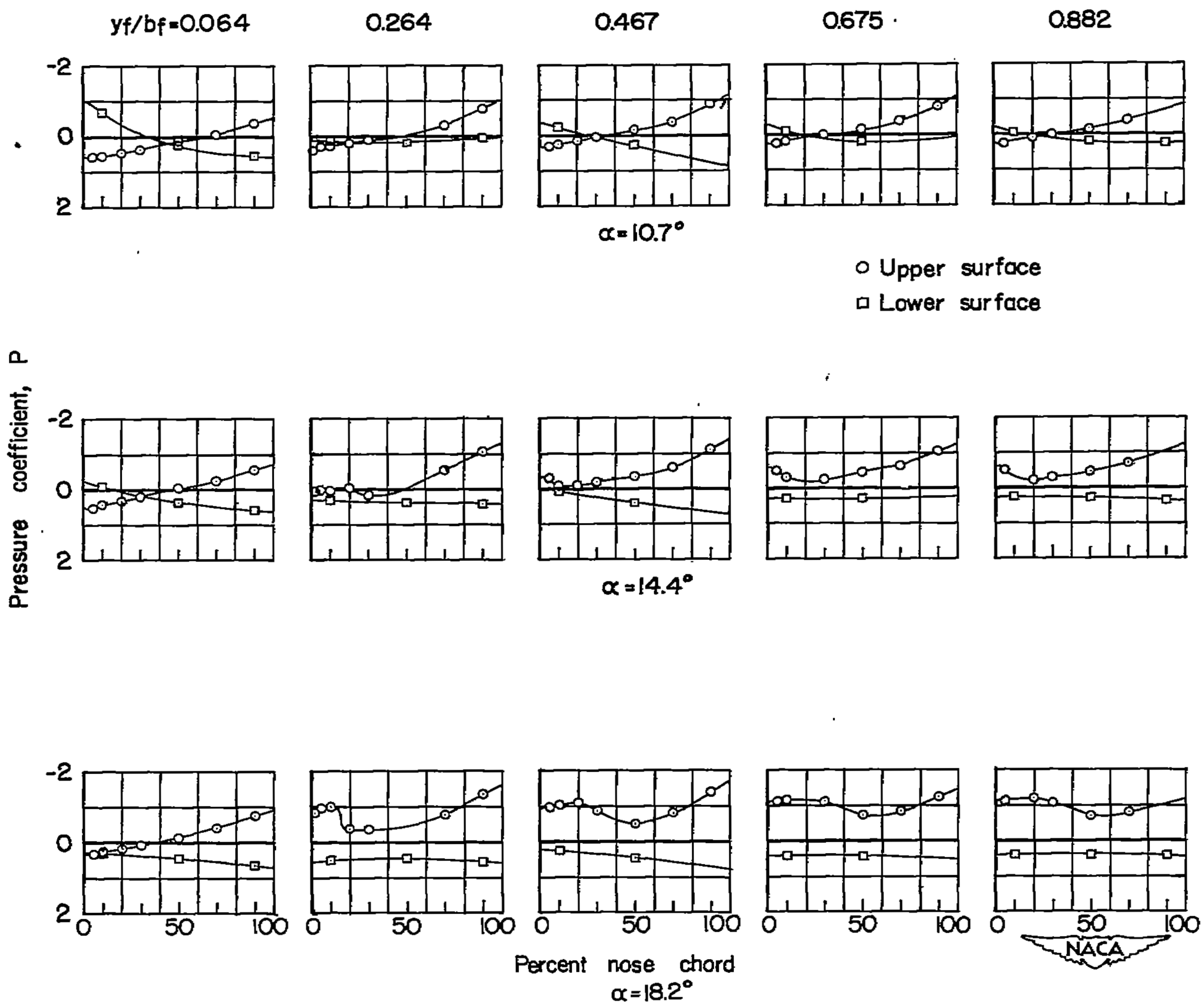

Figure 6.- Chordwise pressure distribution for five spanwise stations. Droop-nose flap deflected 40°.

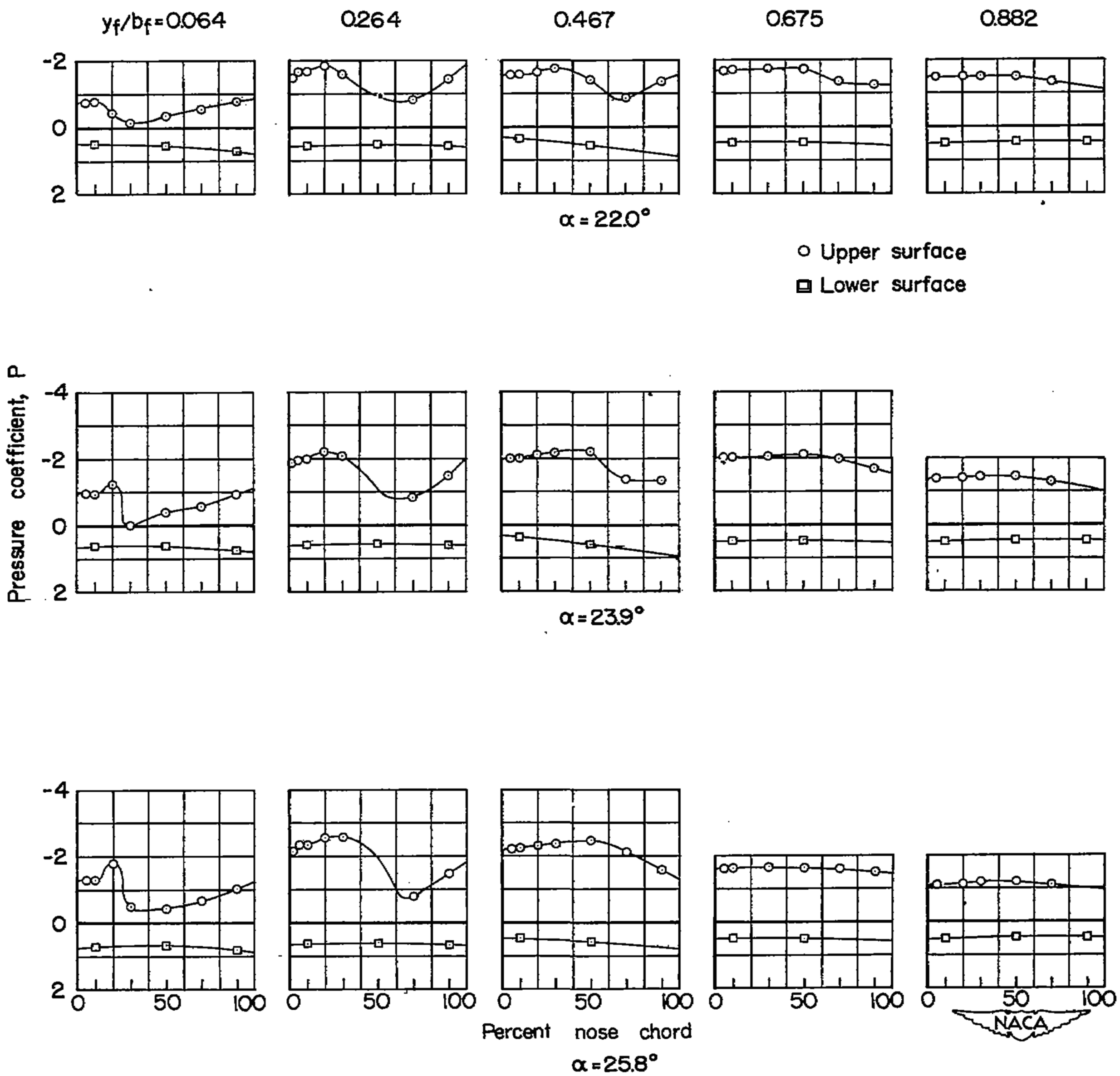

Figure 6.- Concluded.

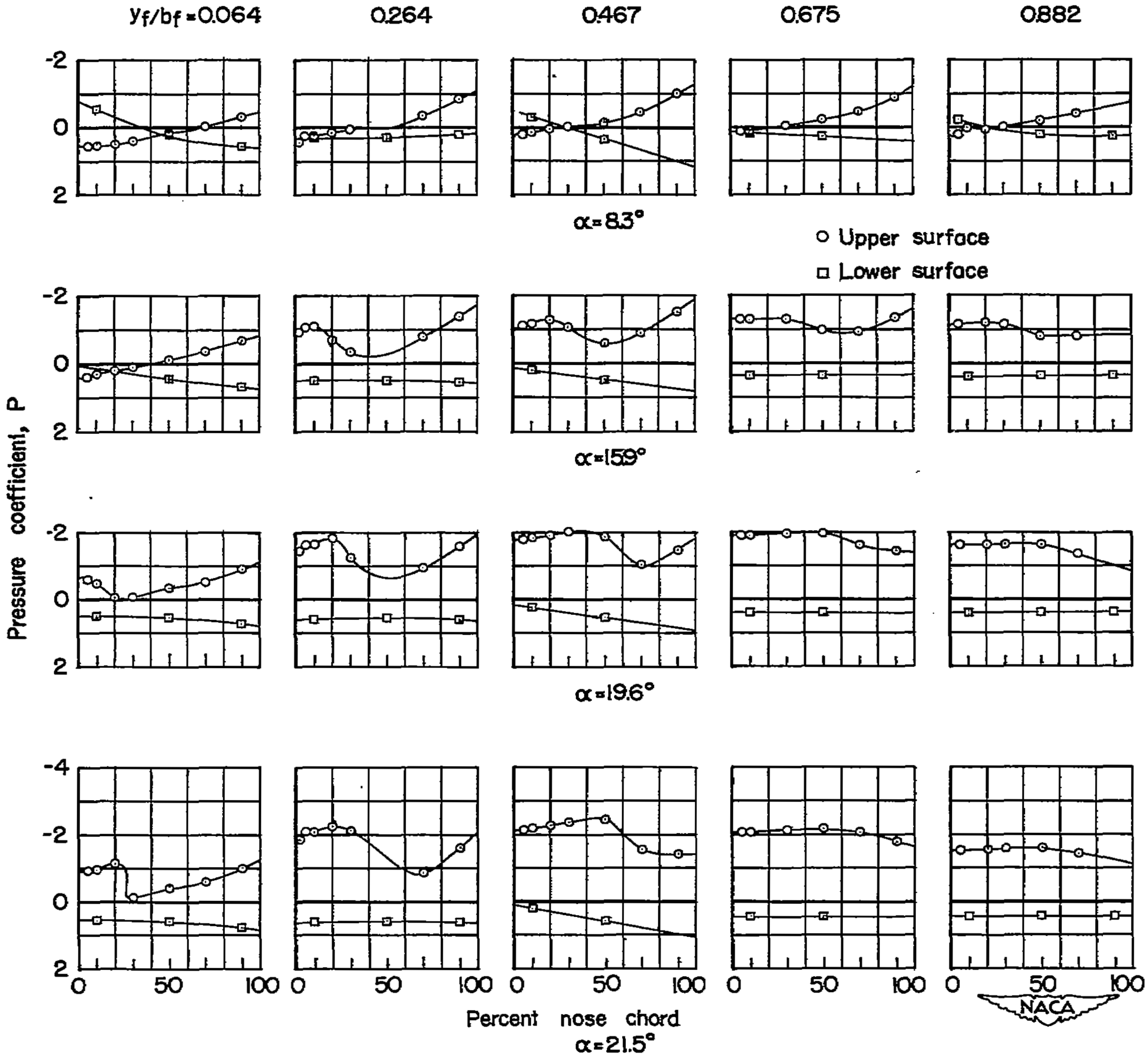

Figure 7.- Chordwise pressure distribution for five spanwise stations. Full-span droop-nose flap and semispan plain flap deflected 40°.

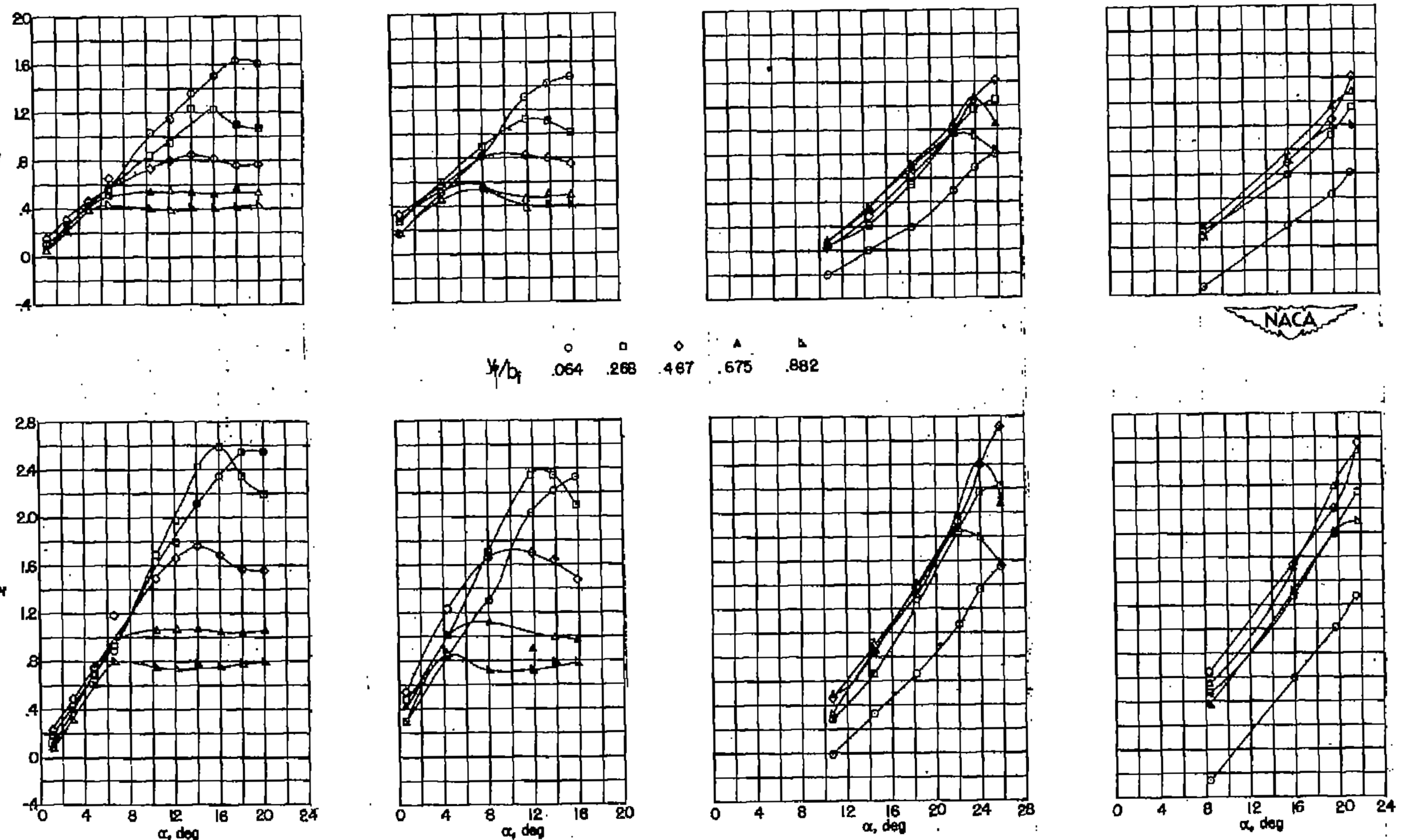

(a) Basic wing.

(b) Semispan plain flap deflected 40°.

(c) Full-span droop-nose flap deflected 40°.

(d) Semispan plain flap and full-span droop-nose flap deflected 40°.

Figure 8.- Variation of section normal-force and hinge-moment coefficients with angle of attack for four configurations.

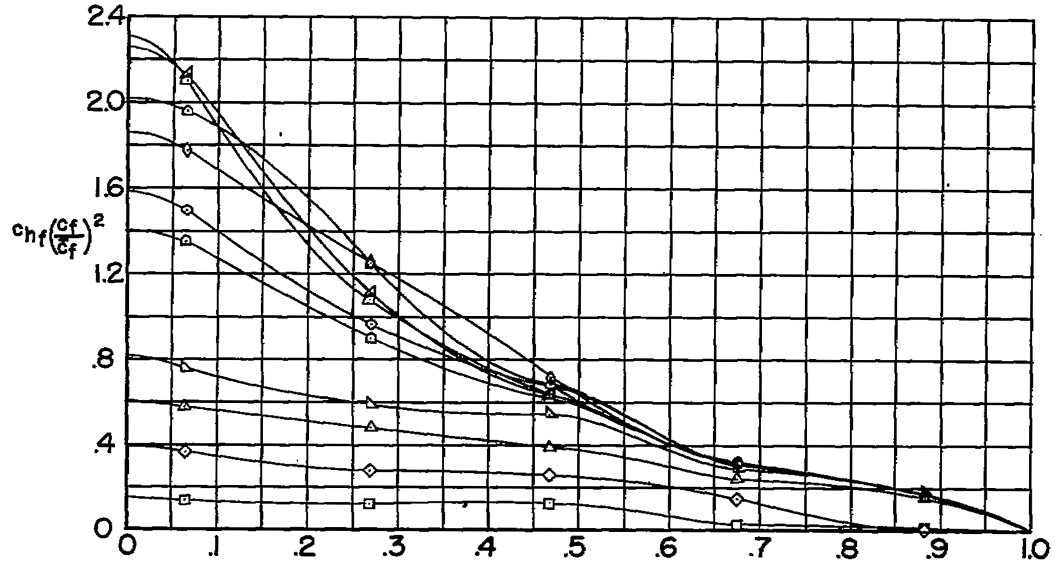

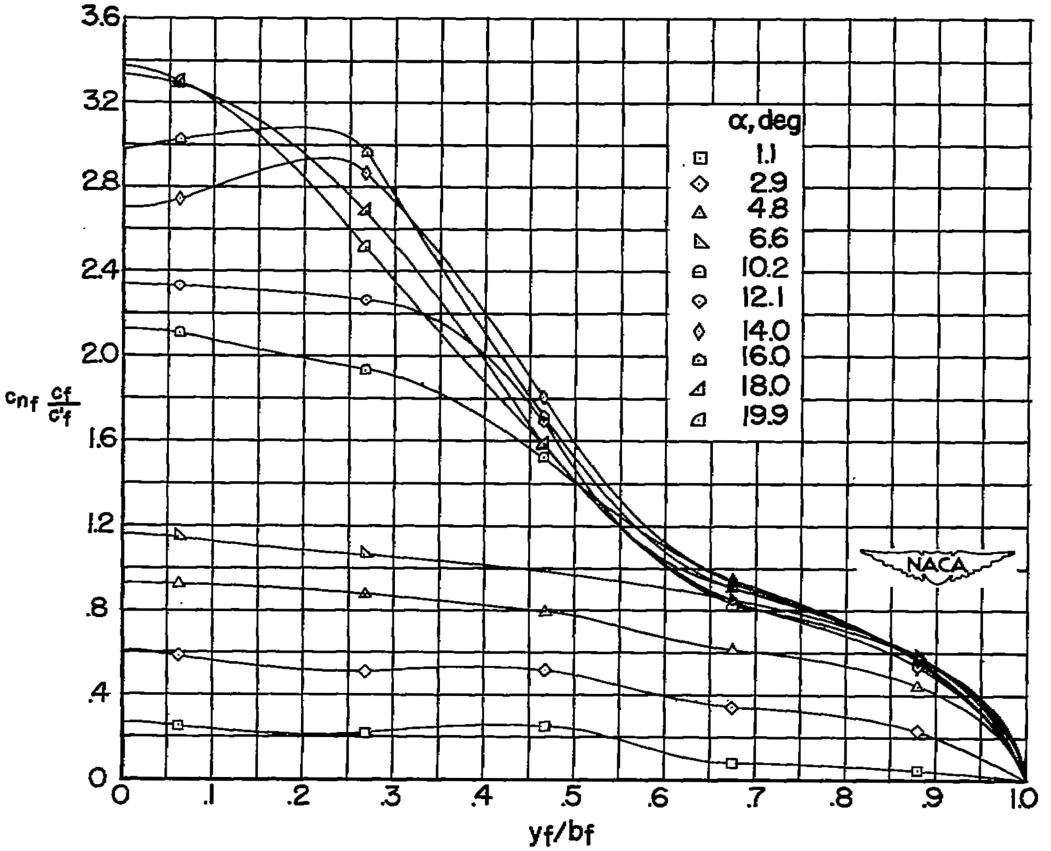

Figure 9.- Spanwise distribution of normal-force and hinge-moment parameter for several angles of attack. Basic wing.

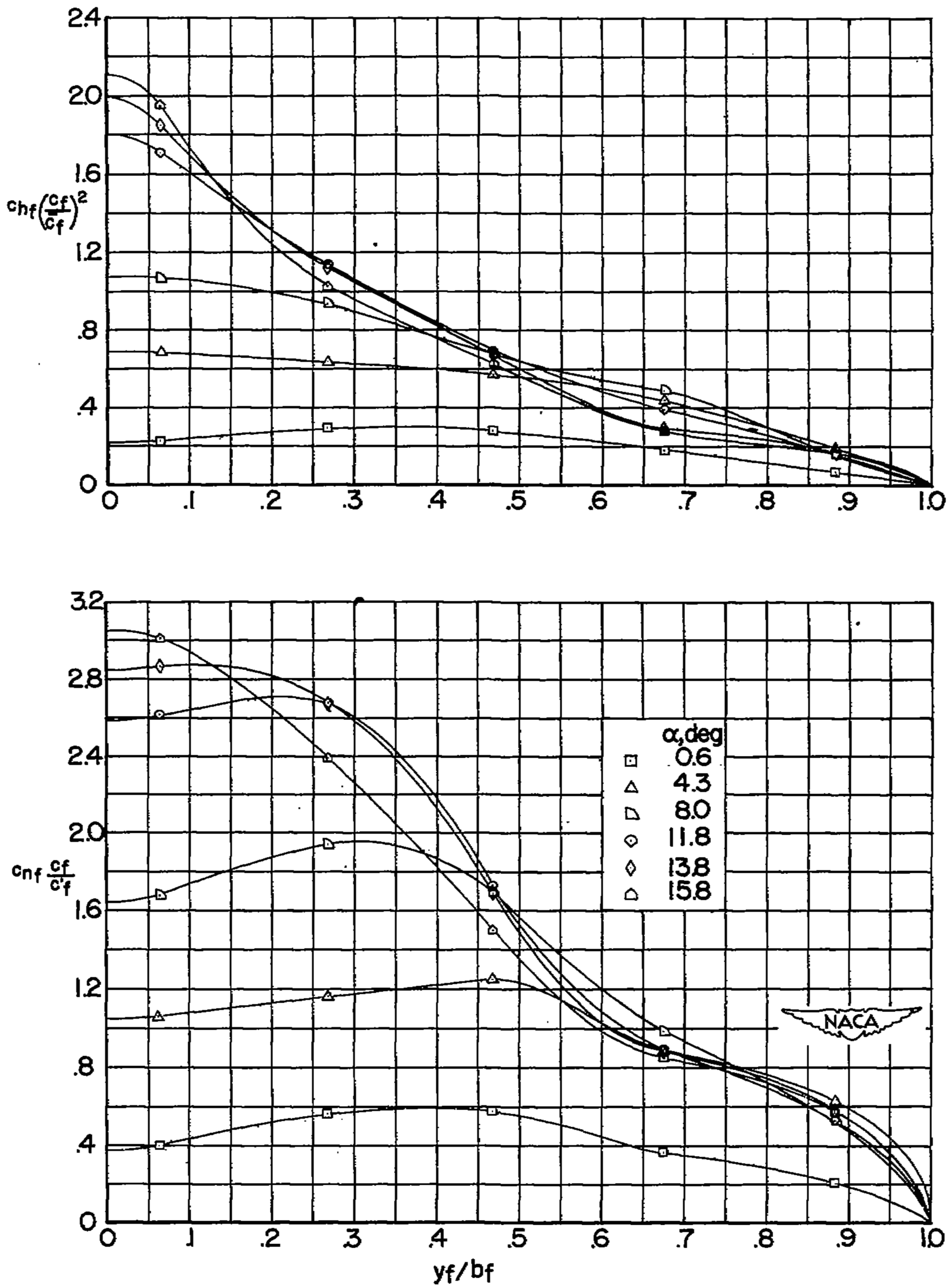

Figure 10.- Spanwise distribution of normal-force and hinge-moment parameter for several angles of attack. Semispan plain flap deflected 40°.

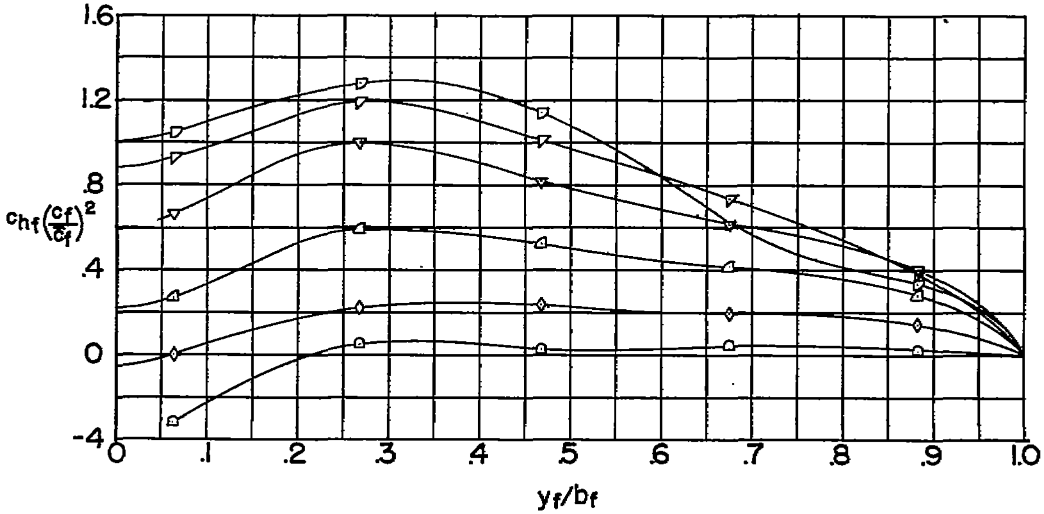

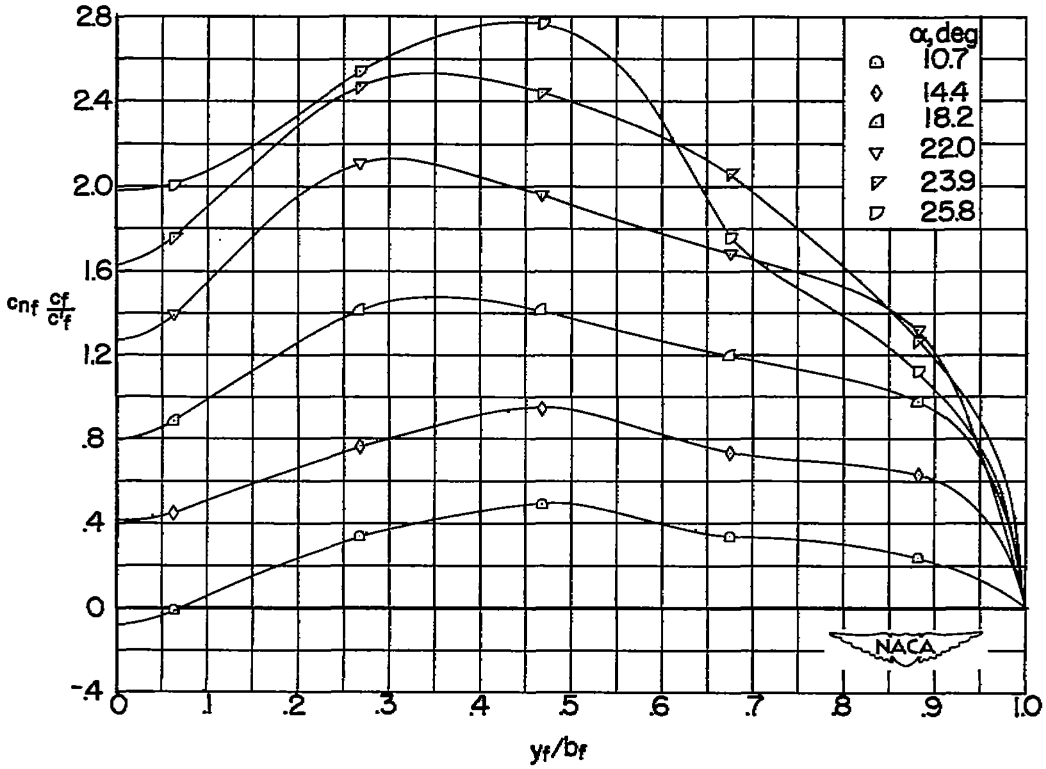

Figure 11.- Spanwise distribution of normal-force and hinge-moment parameter for several angles of attack. Full-span droop-nose flap deflected 40°.

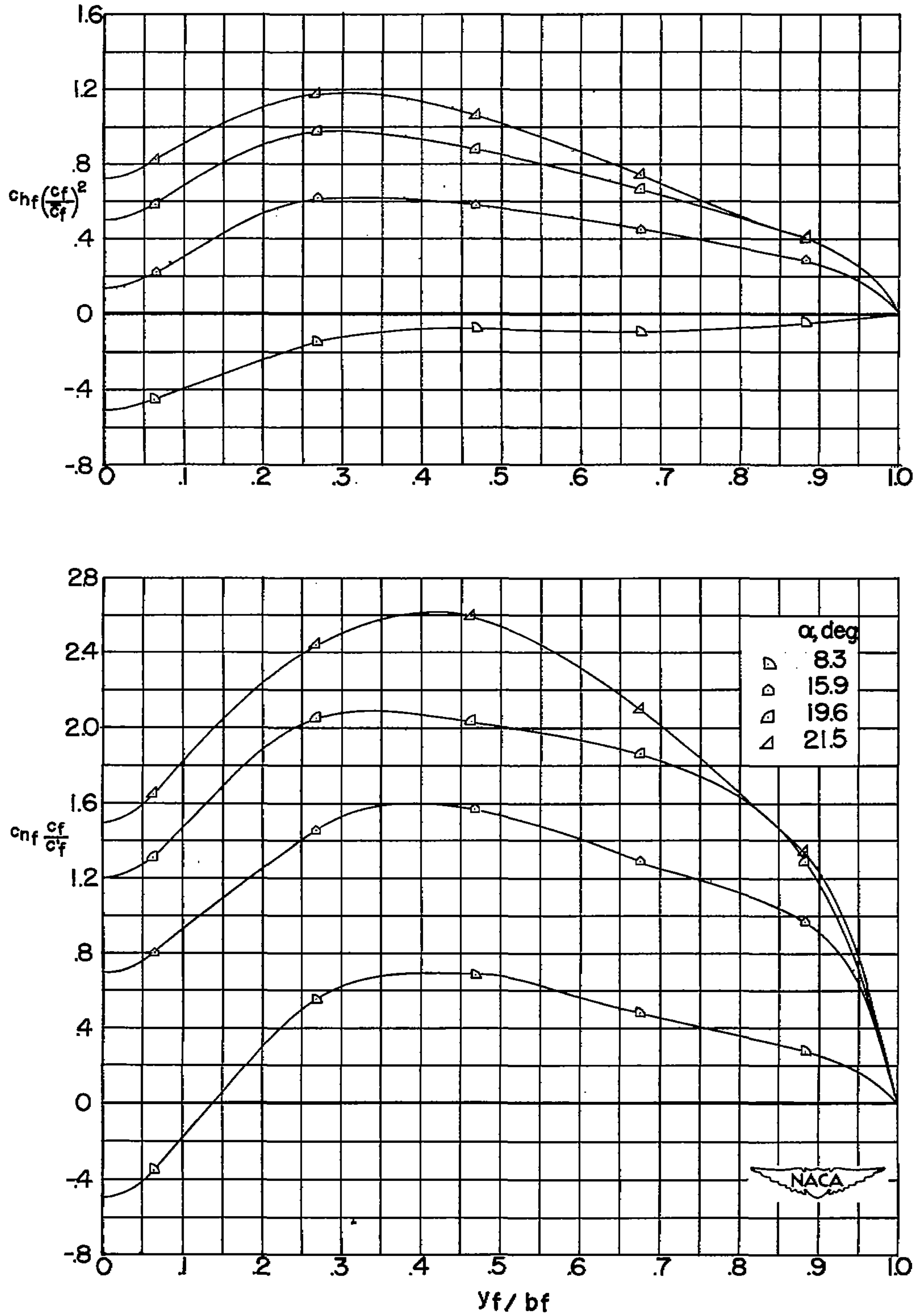

Figure 12.- Spanwise distribution of normal-force and hinge-moment parameter for several angles of attack. Full-span droop-nose and semispan plain flaps deflected 40°.

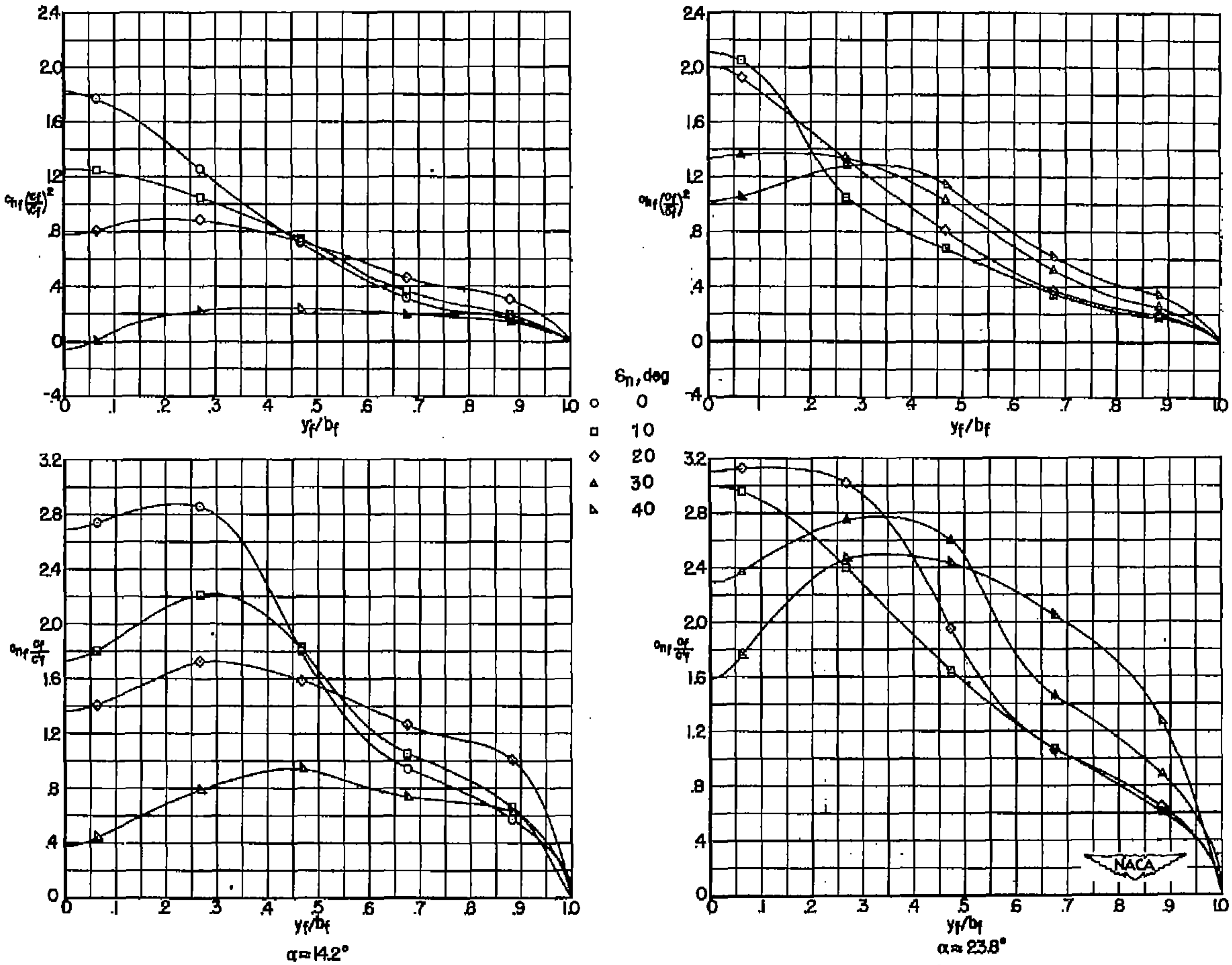

Figure 13.- A summary of the effects of droop-nose flap on the normal-force and hinge-moment parameters.

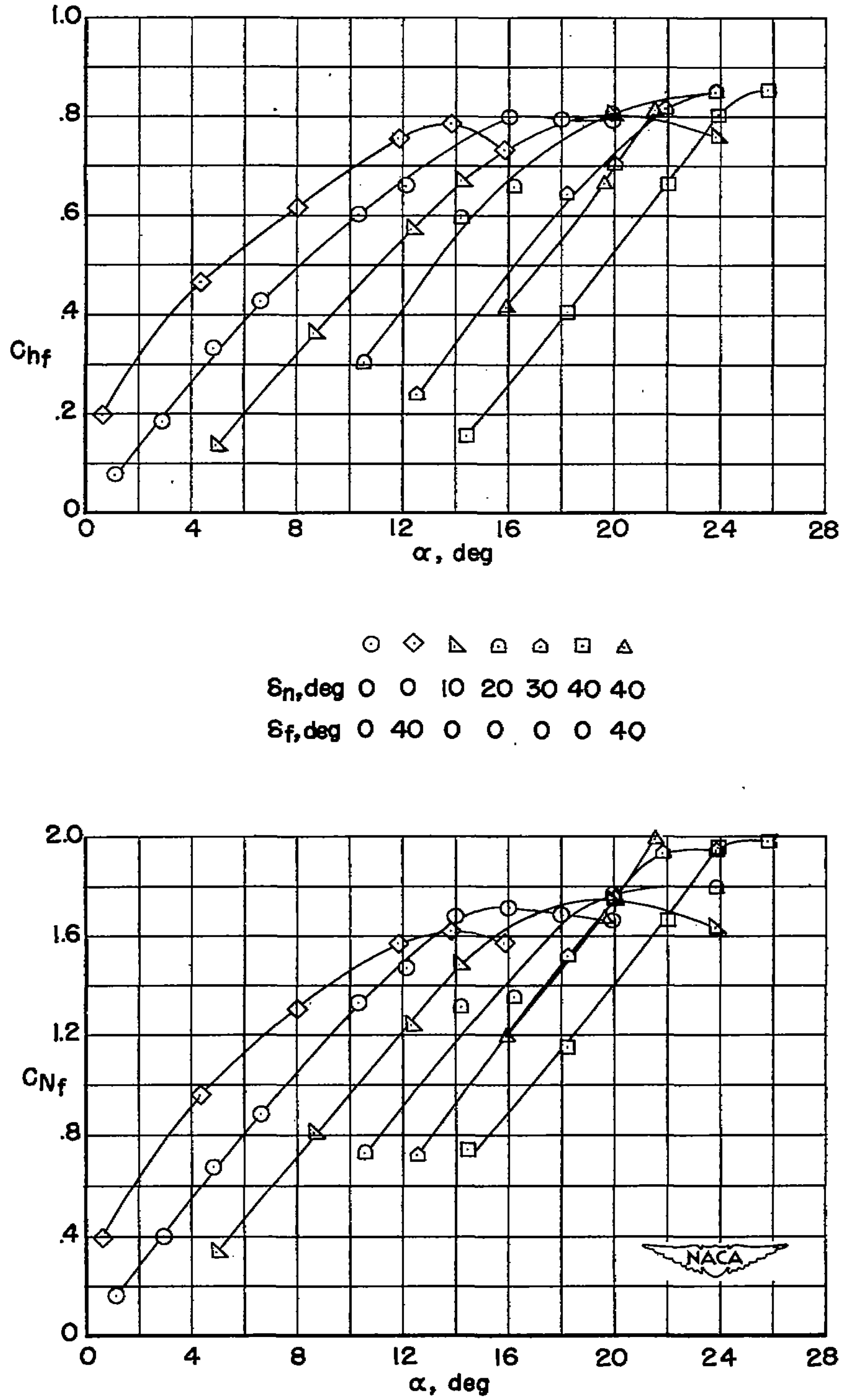

Figure 14.- Variation of normal-force and hinge-moment coefficients with angle of attack for seven flap configurations.

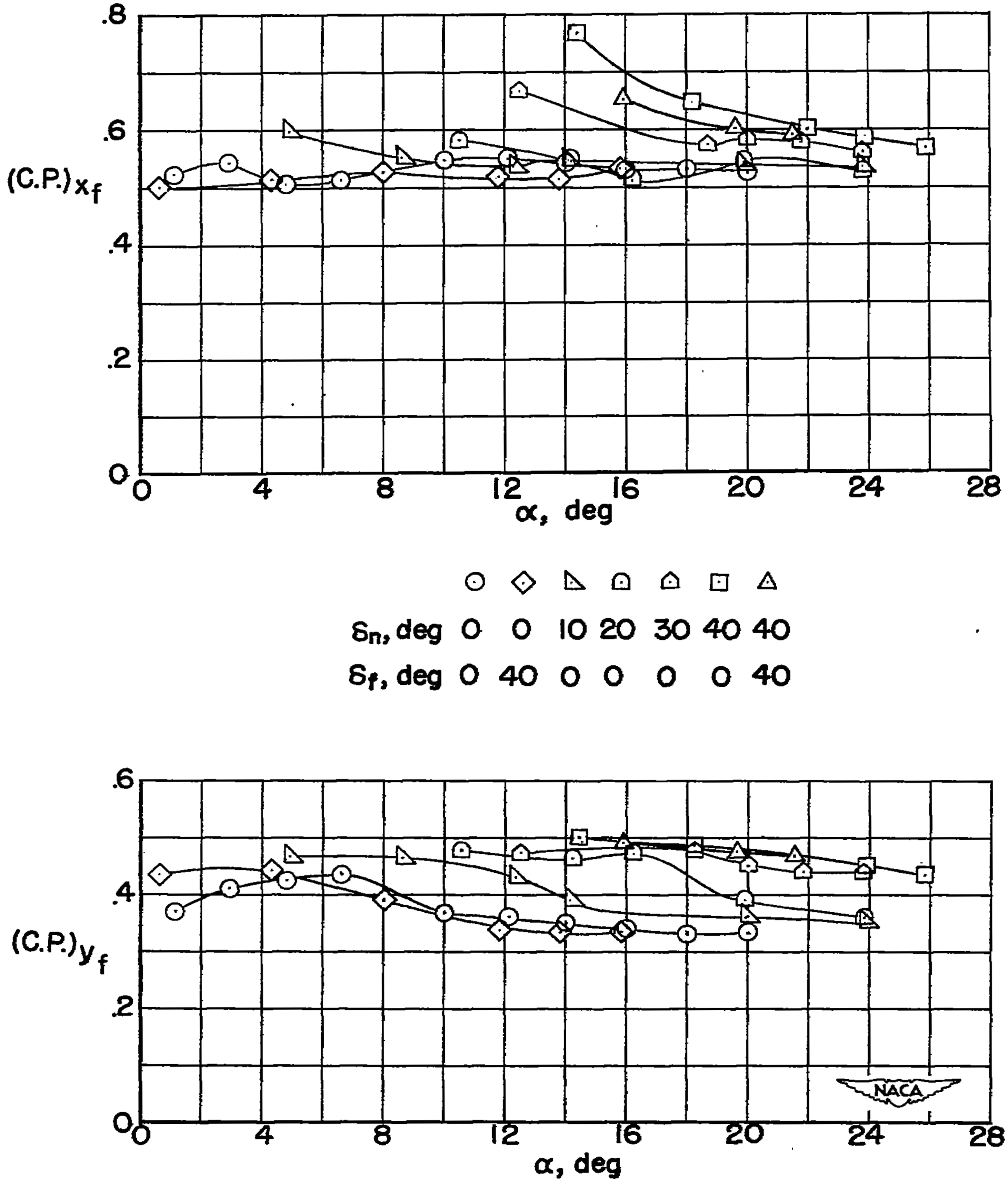

Figure 15.- Spanwise and chordwise variation of center of pressure with angle of attack for seven flap configurations.

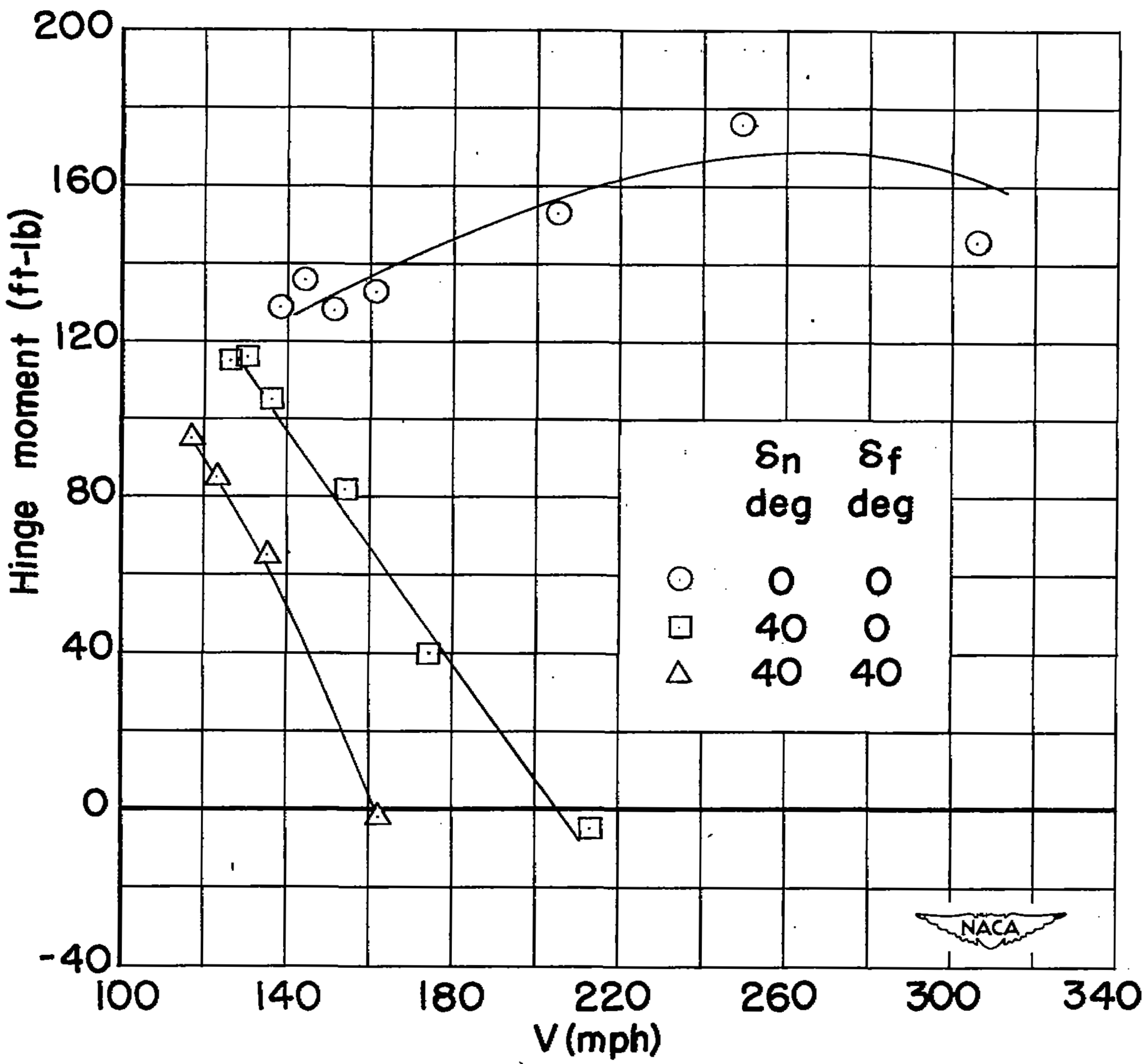

Figure 16.- Variation of droop-nose flap hinge moment with velocity for several likely landing approach configurations.